Spring 5-2022

Design and Analysis of Electrical Power and Communication Systems for 3U SeaLion CubeSat Mission

Joseph D. Siciliano
Old Dominion University, j.siciliano33@gmail.com

DESIGN AND ANALYSIS OF ELECTRICAL POWER AND COMMUNICATION SYSTEMS FOR 3U SEALION CUBESAT MISSION

by

Joseph D. Siciliano
B.S. May 2018, United States Coast Guard Academy

A Thesis Submitted to the Faculty of
Old Dominion University in Partial Fulfillment of the
Requirements for the Degree of

MASTER OF SCIENCE ENGINEERING

ELECTRICAL AND COMPUTER ENGINEERING

OLD DOMINION UNIVERSITY
May 2022

Approved by:

Dimitrie C. Popescu (Director)

Shu Xiao (Member)

Sharan A. Asundi (Member)

ABSTRACT

DESIGN AND ANALYSIS OF ELECTRICAL POWER AND COMMUNICATION SYSTEMS FOR 3U SEALION CUBESAT MISSION

Joseph D. Siciliano
Old Dominion University, 2022
Director: Dr. Dimitrie C. Popescu

Old Dominion University (ODU) Space Systems students in conjunction with the United States Coast Guard Academy (USCGA) are designing and developing a 3U Very Low Earth Orbit (VLEO) CubeSat mission aptly named SeaLion. This work specifically details the design of the Electrical Power System (EPS) and Communication System of the satellite. Electrical power in orbit is a precious commodity and must be carefully regulated and distributed to ensure the satellite's operational health. Commonly, CubeSat electrical power is retained in orbit via outward facing solar cells and stored in onboard rechargeable batteries. This thesis proposes using non-rechargeable primary battery cells and custom hardware to maximize operational time with strict Very Low orbital lifetime constraints. Primary battery cell choice and the encompassing battery power supply design with reliability features are provided. Major functions of the EPS including voltage and current regulation and circuit protection and monitoring are also designed and analyzed for performance and reliability. The communication system consists of two half-duplex radios centered in the UHF and S-Band frequency bands to communicate with the Virginia CubeSat Constellation (VCC) and Mobile CubeSat Command and Communications (MC3) ground station networks, respectively. The design and analysis provided show the viability and cost efficiency of using primary cells and custom and readily available hardware for Very Low Earth Orbit CubeSat missions.

This work is dedicated to my wife Cherokee, who without her strength, love, and encouragement, I would not be the person I am today. I am forever grateful and indebted to her for the unconditional kindness and support she has shown me in pursuit of my academic and professional dreams.

It continually holds true that "no one achieves anything alone."

ACKNOWLEDGEMENTS

I would like to first thank Dr. Shu Xiao for his advice and assistance in power electronic theory and design. Your Power Electronics course and your expertise and guidance helped me tremendously with the formation of the power conversion theory, design, and analysis portion of this work. I would also like to thank Dr. Sharan Asundi for his leadership in this mission and igniting a spark of novelty for this thesis with the introduction of primary battery cells in the power supply. Finally, I would like to thank my advisor, Dr. Dimitrie Popescu, for providing the time, tools, and guidance needed to succeed in wireless communications engineering and formal academic writing.

TABLE OF CONTENTS

LIST OF TABLES

LIST OF FIGURES

Figure Page

CHAPTER 1

INTRODUCTION

Small satellite missions have become increasingly popular in the aerospace industry and academic community for their relatively low monetary costs and complexity. Satellite size in the industry is normally determined by its mass which is deemed to be generally less than 180 kg for small satellites. However, CubeSats generally fall into much smaller size categories of small satellites, most commonly in the nanosatellite range of 1-10 kg. The original idea of the CubeSat was created by Jordi Puig-Suari at California Polytechnic State University and Bob Twiggs at Stanford University to "provide affordable access to space for the university science community." [9] A CubeSat is a cubic satellite with one unit (1U) standard of volume 10 cm x 10 cm x 10 cm with approximately 1 kg mass. To increase the size of the mission, these standard units are stacked together. The Mission SeaLion is a 3U CubeSat with approximately 3.4 kg mass. Figure 1 shows increasing size of CubeSats' units from 1U to maximum 12U in accordance with the CubeSat Design Specification [10].

University led CubeSat missions have increased drastically in recent years. From 1994 to 2017 there have been 344 total documented university led small spacecraft missions with approximately two-thirds of those developed and launched from 2010-2017 [11]. Per [11], these missions had varying purposes including communications, educational, imaging, military, science, and technology demonstration. It is implied in [11] that the introduction of the CubeSat Standard in 1999 led to increases in the sheer number of missions across academia and an overall increase in university mission successes. Closer to home in Virginia is the ThinSat program, sponsored by Virginia Space, Northrop Grumman, and NASA Wallops Flight Facility [12]. ThinSats are another type of small satellite in a smaller form factor bringing them into the picosatellite category. The ThinSat program gives local universities and primary schools in Virginia and surrounding states an opportunity to gain invaluable education and experience from developing a low cost, short term satellite for low orbit missions [12].

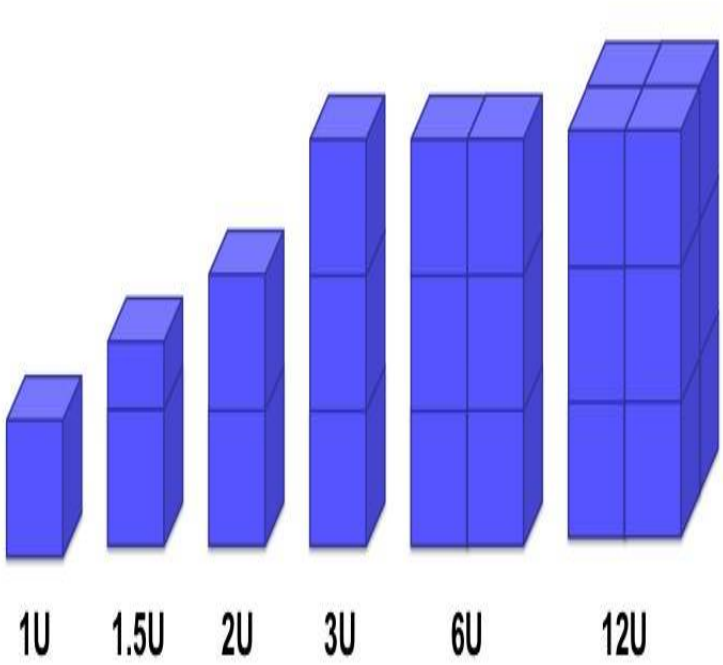

Fig. 1: CubeSat Standard Unit Sizes from [2]

1.1 BACKGROUND AND MISSION

With the high cost of space missions and the typical constrained budgets of nonprofit backed missions including those of universities, often access to only Low Earth Orbit (LEO) altitudes are possible for CubeSats. The first stop for getting access to a launch vehicle for the typical university is NASA through their CubeSat Launch Initiative (CSLI) program. Educational and nonprofit CubeSats through this program are deployed from the LEO International Space Station (ISS). The CubeSat Mission SeaLion, however, is backed by the Virginia Institute For Spaceflight and Autonomy (VISA) and is being carried by Northrop Grumman's Antares (NG-18) rocket from NASA Wallops Island launch facility. With the anticipated Very Low launch altitude from Antares, careful consideration must be given by the SeaLion team engineers to maximize the chance of mission success during the short window. The anticipated VLEO of SeaLion restricts the longevity of the mission and thus brings power design decisions into unique consideration.

The expensive nature of space missions drives innovation in the aerospace industry and in academia. Students and engineers alike are challenged to optimize the mission design to accomplish as much as possible with the resources available. Mission SeaLion gives students

and faculty at ODU and USCGA the ability to generate custom solutions to highly constrained engineering problems. Mission SeaLion enabled this work to provide a custom, cost efficient solution to provide electrical power to the satellite for a limited window of opportunity in orbit. Commercial Off The Shelf (COTS) electrical power systems for CubeSats are inherently complex and expensive. This work shows that a feasible EPS can be designed in-house for a fraction of the COTS cost with careful attention given to the analysis of the chosen components. An overview of the communications design of SeaLion is also provided using existing ground station network infrastructure. To detail Mission SeaLion in full, the mission objectives are listed below from the project's recent Critical Design Review (CDR):

Primary Mission Objectives:

- Mission SeaLion will establish a UHF communication link with Virginia ground stations.
- Mission SeaLion shall validate the operation of the IP as a primary payload.
- Mission SeaLion shall successfully transmit "mission data" defined above to ground stations on Earth.
- Mission SeaLion shall adhere to CubeSat standards as per CubeSat CDS Rev.14.1 [10].
- Mission SeaLion will establish an S-band communication link with the MC3 network of ground stations.

Secondary Mission Objectives:

- Mission SeaLion shall validate the operation of the Ms_S as a secondary payload.
- Mission SeaLion shall validate, on-orbit, the DeCS experiment as secondary payload.

Tertiary Mission Objectives:

- Mission SeaLion shall validate, on-orbit, the deployment and functioning of the custom developed UHF antenna system and its deployment.
- Mission SeaLion shall validate, on-orbit, a satellite bus for very low Earth orbit CubeSat missions, which includes non-rechargeable batteries as the only power source.
- Mission SeaLion shall gather DeCS experiment in-orbit performance data by capturing structural behavior through an accelerometer and temperature sensor.

The mission lifetime of SeaLion was verified via orbital computer simulations in the *Analytical Graphics, Inc.* (AGI) Systems Tool Kit (STK) software. In performing these simulations using STK's Astrogator Propagator, the SeaLion team found that with an orbital inclination of 51.64° and launch altitude of 180 km that the expected mission lifetime would be approximately one week (7 days). At that endpoint, SeaLion would reach its lowest altitude in the orbit, known as the *periapsis*, and then presumably drop out of orbit and burn up in the atmosphere. This relatively short mission lifetime drives the power requirements for SeaLion since we want to maximize the power available to conduct mission operations for the 7 day time frame. An initial estimate of 100-150 Watt-Hours (Wh) was proposed to satisfy the power requirement. However, as the SeaLion design matured, additional components were added to increase general functionality and the likelihood of meeting the mission objectives. These components increased the SeaLion's electrical power consumption and, thus, provided the need for additional power. Figure 2 shows the computer-aided design (CAD) of the whole Mission SeaLion CubeSat at the time of this writing. Additional data required from the orbital analysis is specifically for the design of the radio communications system of SeaLion. We must know the maximum line of sight distance that SeaLion will be from any respective ground stations intended for communications. In an elliptical orbit, the distance from the ground varies tremendously as the satellite passes overhead. This maximum distance experienced from the ground will be crucial in establishing a radio link with SeaLion and thus provides additional performance requirements for the radio hardware design. Figure 3 shows a 3-D view of SeaLion's expected orbit generated from the STK simulations with respect to the two ground stations intended for radio communications.

Fig. 2: Current CAD of Mission SeaLion 3U CubeSat

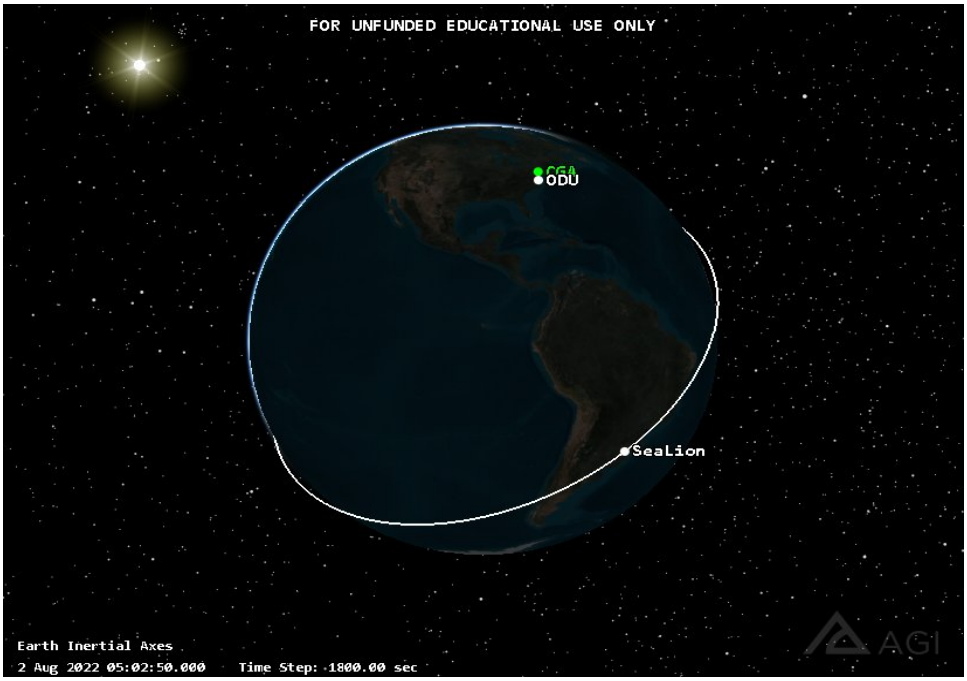

Fig. 3: 3-D Visualization of SeaLion's Expected Orbit via STK Simulation

1.2 THESIS CONTRIBUTION AND OUTLINE

This work introduces the mission concept and the need for an optimal and robust Electrical Power System (EPS) to power the vital components and payload of SeaLion. The novelty of this work lies in the power storage and supply of the system–utilizing primary, non-rechargeable battery cells as the sole source of electrical power for satellite operation. Battery design, power regulation and protection, and communications design choices are explained. Electrical theory and analysis are provided to reinforce SeaLion EPS and communications design decisions. At the time of this writing, SeaLion is planned for launch via NG-18 in August 2022 with a secondary option to launch with NG-19 in April 2023.

With the purpose of this work and Mission SeaLion objectives established in Chapter 1, the technical detail of the design decisions for the EPS and radio communications are then explained. Chapters 2 and 3 encompass the EPS design and analysis for the battery pack power supply and overall circuitry, respectively. Chapter 2 introduces the EPS by first reviewing popular COTS EPS modules and framework and builds the power supply and power converters from the literature. Chapter 3 gives an in-depth analysis to the power conversion and consumption of SeaLion and also includes a wholistic view of the EPS design. The mission power budget is then calculated based on current component and payload selections. Chapter 4 is the communication system design and covers the radio hardware, frequency allocation, and link budget analysis for SeaLion. Chapter 5 concludes the thesis and establishes future work required to realize SeaLion's EPS and communications designs.

CHAPTER 2

DESIGNING THE ELECTRICAL POWER SYSTEM FOR CUBESATS WITH NON-RECHARGEABLE BATTERIES

In order to design and develop our own Electrical Power System, a thorough literature review was conducted on the typical CubeSat EPS design and common COTS EPS hardware utilized in university CubeSat missions. As previously mentioned, the novelty of the comparison between SeaLion's EPS and most published EPS designs is highlighted due to the difference in the power source, choosing primary over secondary batteries as the main power source and avoiding the installation of solar cells and management of solar cell energy.

2.1 CUBESAT EPS REVIEW

Because of the significant size and weight restrictions of the CubeSat design standard [10], electrical power becomes a sought-after commodity for spacecraft operations. The majority of CubeSat university missions use solar panels and (rechargeable) secondary batteries to provide power to the spacecraft's main electrical components including the on-board computer, radio frequency hardware, various sensors, and the main payload. The solar panels' access to sunlight is dependent on type and size of orbit and the spacecraft's physical orientation. With CubeSats small size and limited surface area, this proposes an immediate concern. Coupled with limited attitude control ability, solar panels with rechargeable batteries can significantly detract from the available power the CubeSat can use to operate at any given time post-launch. The cost of solar panels can also drive concern with university CubeSat projects. COTS solar panels sold by aerospace product manufacturers cost thousands of dollars alone. To cover one full length 3U surface (SeaLion's size), CubeSat manufacturers' solar panel approximate prices are listed in Table 1. As seen in the table, solar panel costs to cover all four sides of a 3U CubeSat can run up to ($5,000 x 4) $20,000 [13] which can be a crippling cost for a university project.

TABLE 1: Common CubeSat Manufacturers' Solar Panel Cost in USD

COTS Manufacturer	**Cost in USD**
EnduroSat	$5,100
DHV Technology	$5,000
Pumpkin Space	$5,650

With budgetary constraints and primary mission objectives established, the design decision was made to use primary, non-rechargeable batteries. The main goal of this section, however, is to discuss the design decisions and how the power is regulated, distributed, and monitored for the success of the mission. The hardware of the satellite that performs these tasks is referred to as the Electrical Power System (EPS). As with the solar panels, university missions mostly opt to use COTS EPS units due to their proven reliability and often the simplicity of operation. Many of the COTS manufacturers and providers boast the plug-in-play ability of their EPS units which is attractive to student led mission with limited time and expertise in complex power electronics. Again, the higher prices of these units often match the advantages. Table 2 lists commonly used COTS EPS units and their respective estimated prices.

TABLE 2: Common CubeSat Manufacturers' EPS Module Cost in USD

COTS Manufacturer	**Cost in USD**
EnduroSat	$4,400
Space Inventor Aps	$5,100
Pumpkin Space	$10,500
GOMSpace	$5,000
AAC Clyde Space	$5,000

Two popular COTS EPS units used in university CubeSat missions are the GOMSpace P31u module and the AAC Clyde Space EPS. Old Dominion University's previous CubeSat mission, the *VCC Aeternitas*, utilized the GOMSpace P31u module as their EPS [14]. With this knowledge, and the respective companies' record of successful small satellite missions using these modules i.e. flight heritage, they were used as important references in designing the EPS of SeaLion. The GOMSpace P31u [3] module's power is driven by solar panel input to pure Lithium-Ion rechargeable battery cells. These cells can be customized in multiple configurations, but Aeternitas used the P31u module with two Li-Ion 18650 cells in parallel. The popular OPTIMUS [15] battery module from AAC Clyde Space offers a singular 30-, 40-, or 80-Wh Li-Ion cell as a rechargeable power source to use in conjunction with their EPS module. Since the title name EPS refers to the whole electrical power system of the satellite, we consider the combination of the batteries and the power regulation and distribution electronics to encompass the onboard EPS. The COTS EPS modules highlight important features that provide users with safe and reliable power during the mission. Four key features were used to design SeaLion's EPS:

- Multiple voltage regulated power buses
- Communication standard and ability for power monitoring and control
- Overcurrent/overvoltage/undervoltage (OC/OV/UV) protection
- Separation and Remove Before Flight (RBF) pin switches.

These features are necessary to include in a satellite EPS to ensure power generation, regulation, and delivery to vital systems including the On-Board Computer (OBC), radios and communication systems, various sensors, and the mission payload. These four main features will be described in detail for the SeaLion design and compared to the P31u module and Clyde Space EPS.

The GOMSpace P31u module functional block diagram, extracted from [3] and shown in Figure 4, features many additional abilities, but the main four highlighted before are present. The P31u module contains 3.3V and 5V regulated buses along with a raw battery output line, V_{BAT}. The chosen communication standard for monitoring and control is the popular Inter-Integrated Circuit (I2C) standard. OC protection, RBF pin, and power kill switches are present as well. The Clyde Space EPS functional block diagram, provided in [4],

is displayed in Figure 5 and possesses the same attributes which can be seen in the diagram. The "Switch Configuration" block gives the user the ability to specify the RBF and/or separation switches in the circuit [4]. The analysis and comparison of these two modules gives the blueprint for designing a CubeSat EPS. Electrical charge needs to be generated and stored, drawn from the raw power source, then safely regulated and delivered to the load. The load in this context includes the computer, radios, and other vital electronics that make the CubeSat functional. The next section provides a detailed explanation of the design for the onboard electrical power supply.

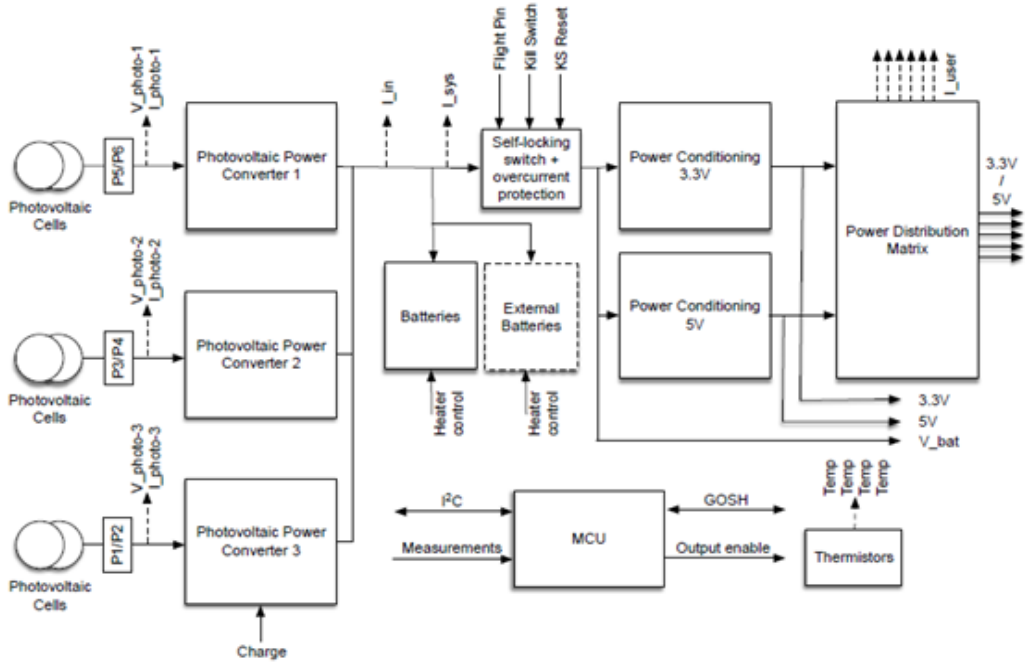

Fig. 4: GOMSpace P31u EPS Module Functional Block Diagram [3]

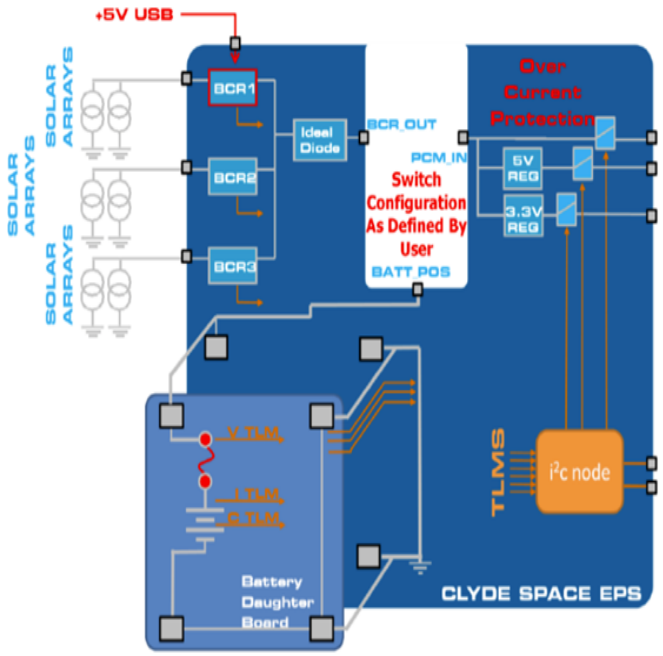

Fig. 5: AAC Clyde Space EPS Module Functional Block Diagram from [4]

2.2 POWER SUPPLY DESIGN

How to Choose a Power Supply: Like many design choices for a satellite mission, this is a intricate and multi-faceted question. The starting point for this design choice is power level and mission duration [5]. Before any electronics were chosen, the SeaLion team knew its expected launch altitude and trajectory and therefore knew its expected viable mission duration. With a Very Low Earth Orbit launch altitude and trajectory, the SeaLion team was able to determine that a realistic mission duration was 5-7 days. For a full treatment of SeaLion's launch trajectory and orbital analysis, see the mission CDR. With this information, we can use Figure 6 from [5] to narrow down the power source selection.

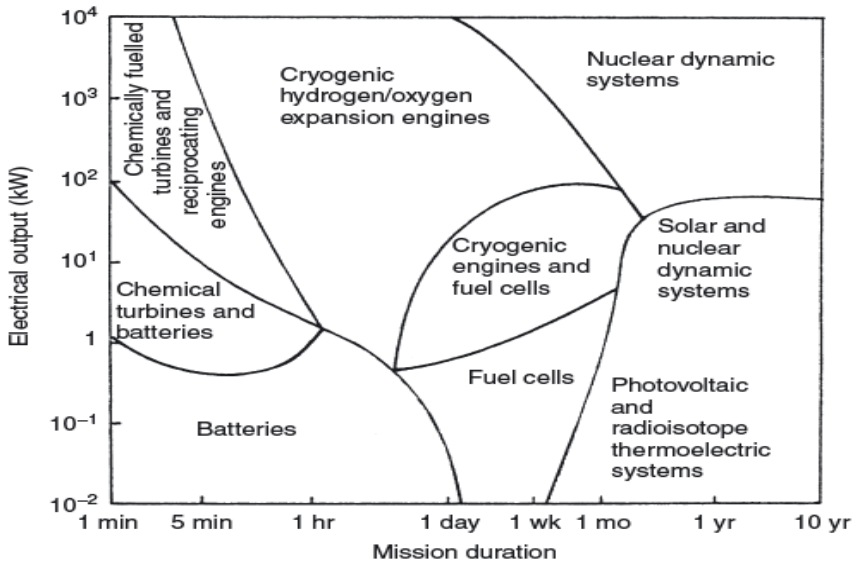

Fig. 6: Electrical Power Output vs. Mission Duration for Power Design Planning from [5]

With mission duration falling in the 1 day to 1 week range and an initial estimate power output estimation of 100-150 W, this leaves SeaLion between batteries and fuel cells as the main power source. The high cost [16] and complexity [1], [5], associated with fuel cells simplified the decision to use batteries as the primary power source. Batteries present a neat and compact way to store energy in a CubeSat since the available volume and weight to utilize onboard is highly restricted. However, with battery cells in mind, Larson and Wertz's *Space Mission Analysis and Design* recommends considering these three main characteristics and their associated requirements and limitations when designing energy storage

for a spacecraft [1]:

- Physical – Size, weight configuration;
- Electrical – Voltage, current load, duty cycles, storage time;
- Programmatic – Cost, mission, reliability.

In already satisfying the programmatic requirements by analyzing mission duration and cost, we will now focus on physical and electrical constraints and requirements.

There are two types of battery cells that can be used as an electrical power source: primary and secondary battery cells. Primary batteries are non-rechargeable, meaning they convert chemical energy into electrical energy but cannot reverse that process [1]. Secondary batteries are rechargeable, meaning that after they discharge, electrical energy can be converted and stored back into the cell as chemical energy. CubeSat missions with longer intended operable lengths utilize secondary battery cells that are constantly recharged by solar panel absorbed energy. Since long term use with solar panels is not necessary with the short mission duration, the main characteristic to consider in choosing a primary or secondary battery cell becomes the specific energy. The specific energy of a battery cell is the direct result of the physical size and chemical makeup of the cell. To calculate the specific energy of a battery cell, the following equation (1) is used.

$$Specific\ Energy\ (\frac{Wh}{kg}) = \frac{Energy\ Capacity\ (Wh)}{Cell\ Mass\ (kg)} \tag{1}$$

The specific energy is the defining parameter in choosing an optimal battery cell for a power supply. A larger specific energy value indicates an increased amount of electrical charge stored per unit of mass of the cell, meaning the cell is providing more charge for its weight and size in comparison. This is crucial in the design phase when trying to maximize power available while minimizing mass and volume additions to the CubeSat. The specific energy parameter was the deciding factor for choosing to use primary cells over secondary cells in SeaLion's power design. Figure 7, provided in [6], shows common cell chemical makeups and their typical specific energy for expected operating temperatures.

From Figure 7, the primary lithium based battery cells provide higher specific energy than any of the secondary rechargeable battery cells, thus making the decision to use non-rechargeable cells easy. Primary cells typically have higher specific energies and therefore should be chosen when recharging is not a viable option. The energy capacity from (1)

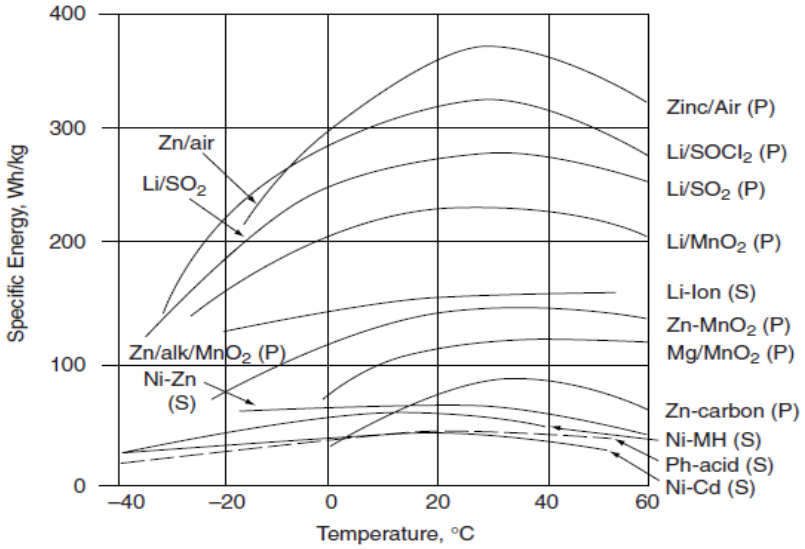

Fig. 7: Specific Energy vs. Temperature in typical Primary (P) and Secondary (S) cells from [6]

is calculated from the nominal (average) voltage and charge capacity of the cell which are determined by the cell size and chemistry. These values should be readily available in the manufacturer's datasheet for the battery. Using (2), we solve for the Energy Capacity (Wh).

$$Energy\ Capacity\ (Wh) = Nominal\ Voltage\ (V) \times Charge\ Capacity\ (Ah) \qquad (2)$$

This is the total electrical energy the battery cell has in store to deliver to an electrical load. To choose a battery with a high energy capacity and specific energy we had to identify chemical makeups that provided both. Table 3, extracted and compiled from [1], shows common primary battery cell chemistry makeups and their respective specific energy ranges.

Table 3 shows the prowess in Lithium based battery chemistry for providing the highest value in specific energy density. This is due to the fact that Lithium has the highest standard potential (voltage) value in magnitude at -3.01V when acting as a reducing agent [17]. For full details of the electrochemical process of Lithium and other metals for primary cells, see [6], [17]. Since using primary cells in space missions as the primary source of power is not very common, popular COTS space vendors do not manufacture or sell these. Thus, we only found two manufacturers that fit the requirements of SeaLion's proposed EPS. EaglePicher Technologies had two viable models, and UltraLife Corporation had another. Utilizing the

TABLE 3: Primary Cell Chemistries and Specific Energy Adapted from [1]

Chemistry	**Sp. Energy (Wh/kg)**	**Application**
Silver Zinc	60-130	High rate, short life
Lithium Thlonyl Chloride	175-440	Medium rate, moderate life
Lithium Sulfur Dioxde	130-350	Low/medium rate, long life
Lithium Monoflouride	130-350	Low rate, long life

manufacturer datasheets [7], [18], [19], and (1), (2), the electrical parameters of each battery cell were calculated in Table 4.

TABLE 4: COTS Available Primary Battery Cells and their Core Parameters

Manufacturer/Model	**(Wh/kg)**	**(V)**	**(Ah)**
EaglePicher/LCF-143	396	2.5	16
UltraLife/UHR-XR34610	424.77	3	16
EaglePicher/LCF-137	524	2.95	16

The UltraLife UHR-XR34610 cell was chosen for SeaLion since it has the highest nominal voltage of the three and a high resulting specific energy density. The nominal voltage is important since it leads to a higher total energy capacity when the cells are configured appropriately in a battery. The UltraLife UHR-XR34610 cell has a Lithium Carbon Monofluoride/Manganese Dioxide (Li-CF_x/MnO_2) chemistry. Li-CF_x and its hybrid chemistries are becoming increasing popular in portable power technologies such as radio equipment, medical devices, and aviation applications [20], [21]. This is due to their significant advantages in high specific energy, wide operating temperature range, and low discharges rates resulting in increased durability and reliability in harsh environments [22]. The U.S. Army has even developed their own Li-CF_x/MnO_2 battery pack to power radio communications equipment for use by soldiers on the battlefield [23]. According to the Li-CF_x/MnO_2 UltraLife Application Guide [20], these Li-CF_x/MnO_2 hybrid cells "deliver 40% or more capacity" than a

sole Li-MnO_2 cell of the same size or lesser in mass. The chosen UltraLife UHR-XR34610 cell is shown below in Figure 8 and its characteristics are listed in Table 5.

Fig. 8: UltraLife UHR-XR34610 Primary Cell from [7]

TABLE 5: UltraLife UHR-XR34610 Primary Cell Characteristics

Model (UltraLife)	UHR-XR34610
Size (Height x Diameter)	60.45mm x 34.01mm
Nominal Voltage	3.0V
Charge Capacity	16 Ah
Energy Density	424.77 Wh/kg
Mass	113g
Operating Temp.	-30°C to 55°C

The next step in the power supply design discussion is to explain how battery cells are configured to increase voltage, current capacity, and ultimately energy capacity. As mentioned before, we have a minimum requirement of 100-150 Wh for the power supply with now a newly proposed target of approximately 350-400 Wh for redundancy and extending the mission length of SeaLion's operation. There is also a minimum voltage requirement of +5V to ensure all electronics onboard have a sufficient voltage supply. To obtain these target numbers of power and voltage, the cells must be configured carefully to increase both the voltage and capacity of the entire power supply. First, we needed to set a target number for voltage with our 5V requirement. This requires the design to increase supply voltage from a single cell of 3V to more voltage by using multiple cells. We know this is possible from Kirchoff's Voltage Law (KVL) which says the sum of individual voltage sources in series is zero for a closed loop circuit. Knowing voltages add together in series from KVL, we can place multiple battery cells in series to add their voltages and increase the total voltage of the battery pack. Mathematically, KVL is given in (3) for n number of cells each with voltage V_c in a loop.

$$\sum_{c=0}^{n} V_c = 0 \tag{3}$$

From [6], [20], we know temperature and discharge time both affect the voltage level of a battery cell; thus, we have to account for these losses. Utilizing the manufacturers' cell testing results from [7] in Figure 9, we can see voltage drops as the cell experiences lower temperatures.

To account for these temperature and discharge time losses, we set the target voltage at 12V for total battery pack design supply voltage. With the UltraLife cell nominal voltage of 3V, the total number of required in series cells [24] is calculated by (4).

$$\frac{V_p}{V_c} = number\ of\ cells\ in\ series \tag{4}$$

where V_p is the total battery pack voltage at 12V. This results in needing four cells in series to get to 12V total. Figure 10 shows the resulting four cells in a series connection summing up to 12V total for the pack output.

Now that the voltage requirement is satisfied, the overall power supply goal of 350-400 Wh needs to be attained. This is accomplished by increasing the charge capacity (Ah) of the battery pack by connecting battery cells in parallel. From Kirchoff's Current Law (KCL), the sum of the electrical currents entering and exiting a node is zero, given mathematically by (5)

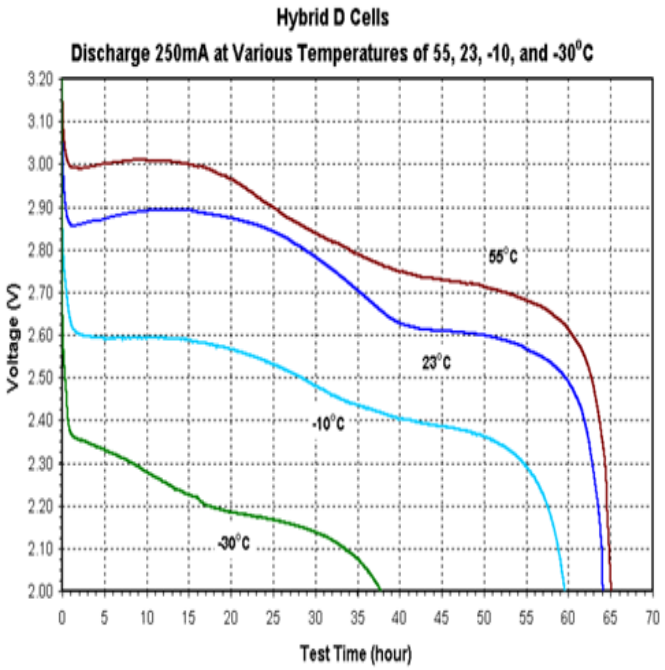

Fig. 9: UltraLife UHR-XR34610 Cell Voltage Vs. Time at Varying Temperatures at 250 mA Discharge from [7]

$$\sum_{c=0}^{n} i_c = 0 \tag{5}$$

where n is the number of currents entering or leaving the node and i_c is the current. Following KCL, parallel currents in a circuit can be summed; thus, the charge capacities of parallel battery cells are summed. Figure 11 shows the equivalent charge capacity for two 16 Ah battery cells in parallel.

Now with the four cells in series required from (4), an additional four 3V-cells in series need to be placed in parallel with the original four in order to increase the charge capacity and, thus, the total energy capacity of the battery pack. With four series cells combined in parallel with another four series cells, the total energy capacity is now calculated in (6) using (2).

$$12\ (V) \times 32\ (Ah) = 384\ (Wh) \tag{6}$$

and the 384 Wh power supply total is in our target range of 350-400 Wh and, thus, our power supply output is finalized. The resulting supply circuit for the cell configuration is a 4-Series 2-Parallel (4S2P) shown in Figure 12.

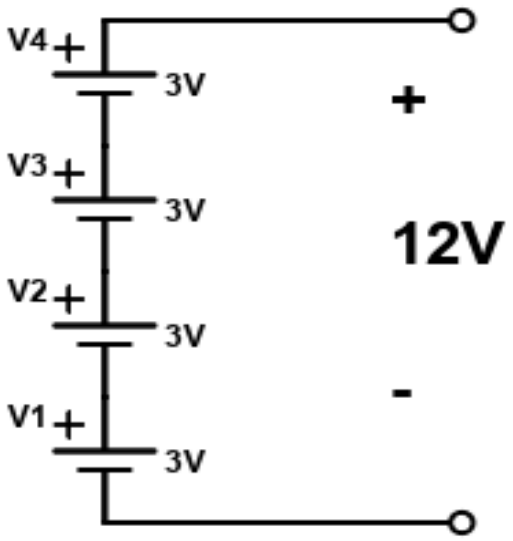

Fig. 10: Four 3V Battery Cells in Series

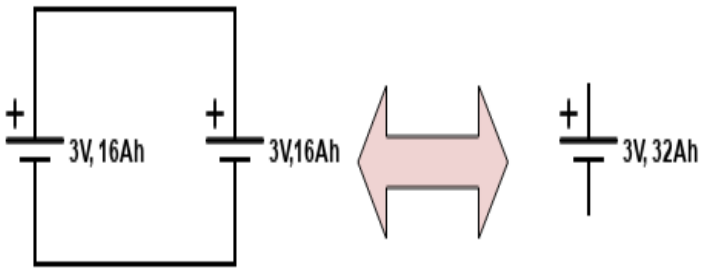

Fig. 11: Two Battery Cells in Parallel to Increase Charge Capacity

2.3 BATTERY FAILURE MODES AND PROTECTION

Precautions and careful considerations must be discussed when connecting primary battery cells together to achieve greater output parameters. The main concern of primary cell connections is unintentionally recharging a primary cell. Some additional common causes of battery failure listed by the Handbook of Batteries [6] are

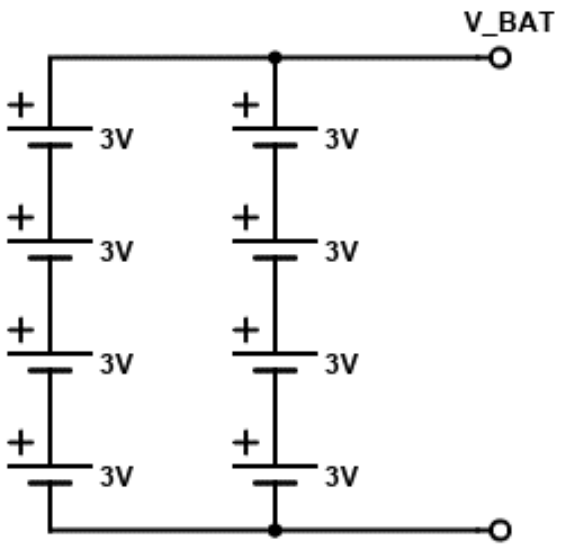

Fig. 12: 4S2P Battery Cell Configuration for SeaLion

- Short-circuiting of battery terminals,
- Excessive high rate of discharge or charge,
- Voltage Reversal.

Each will be verified and discussed in this battery pack design. First, primary cells should never be recharged as it could lead to material leakage or explosion. According to the UHR-XR34610 cell Safety Data Sheet (SDS) [25], "charging a primary cell or battery may result in electrolyte leakage and/or cause the cell or battery to flame." Fortunately, there are specific design elements in battery design that can be put in place to prevent this issue. Diodes should be placed at the front of each series stack to block charging currents between stacks. The diode criteria [6] for this purpose are as follows:

TABLE 6: 1N5822 Schottky Diode Characteristics

Charge Protection Diode Criteria	**1N5822 Parameters**
Forward Voltage Drop	0.525 V
Peak Inverse Voltage	40 V
Forward Current Rating	3.0 A

- Forward voltage drop be small as possible,
- Peak inverse voltage should be rated at twice the voltage of the series stack,
- Forward current rating should be a minimum of

$$I_{min} = 2\frac{I_{op}}{N} \tag{7}$$

where I_{op} is the device operating current and N is the number of parallel stacks. Selecting the Schottky type diode 1N5822 with parameters listed in Table 6 met each of these criteria.

The forward voltage drop is low while peak inverse voltage, 40V, is more than twice the total voltage of a series stack, 12V. The forward current rating is equal to the minimum current described in (7) for the anticipated load of the system. These diodes placed at the front of the series stacks are often referred to as *blocking* diodes due to their function of blocking the lead cell from external charge. The next failure mode to address is battery terminal short circuiting. This is prevented in SeaLion's design by using a nonconductive material to house the battery cells. This failure can also be minimized with the activation of the thermal fuse at the cell terminal installed by the manufacturer [7]. This can keep the cell from exploding or destructing if a short occurred and the internal temperature rose sharply. This unintended catastrophic rise in battery cell temperature is known as thermal runaway. The thermal fuse is also a safety net for the next concern of excessive high rate of discharge.

In an addition to a short circuit, a cell discharge greater than rated parameters can lead to thermal runaway as well. This risk of excessive discharge is mitigated by ensuring the battery pack is not overloaded in the overall design as well as including protection circuitry. There are two forms of overcurrent protection circuitry placed before the payload electronics that are designed to prevent the current from surpassing 3.0 A. The details of

those protection circuits will be discussed in later sections. To verify the battery pack design against overload concern, this 3.0 A maximum for discharge is well within the rated parameter of the up to 7 A for the UHR-XR34610 cell [7].

The last failure mode of voltage reversal could lead to any of the previously listed failures including primary cell charging, thermal runaway, and excessive discharge. Cell voltage reversal is when the lowest capacity cell in a series stack is discharged fully before the others and becomes depleted, reaching 0V [6]. Any further discharge of the depleted cell can result in the voltage reversing to negative which will build up heat in the cell and can cause cell leakage and rupture. This can be prevented by adding parallel diodes to each cell in the series stack. When the voltage of a cell reaches 0V, the diode will conduct and divert the current from flowing through the depleted cell [6]. For this role of bypassing current around the cell, these diodes are referred to as *bypass* diodes in battery design. Incorporating these parallel or bypass diodes into the battery design, SeaLion's final power supply design is complete and shown in Figure 13.

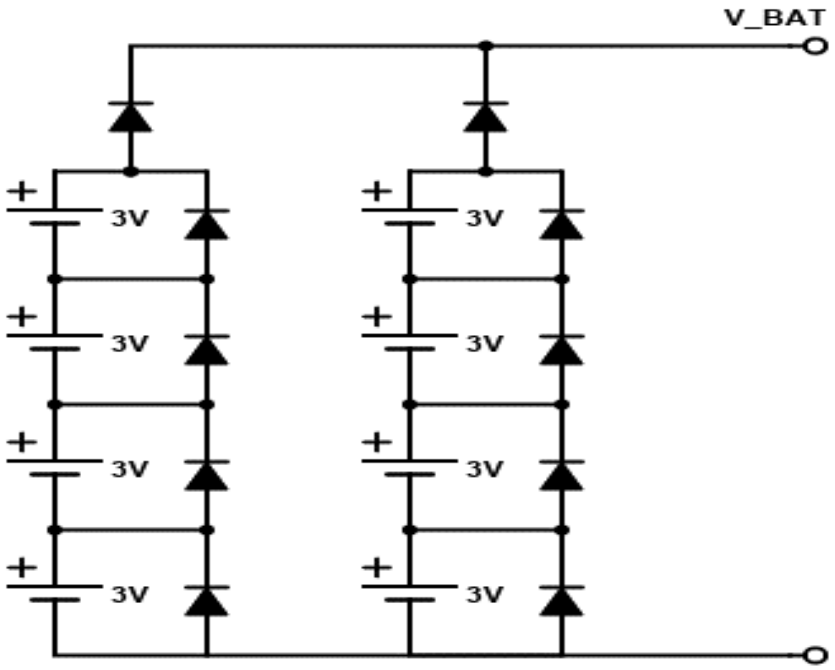

Fig. 13: Final SeaLion Battery Design with Blocking and Cell Bypass Diodes

2.4 VOLTAGE REGULATOR THEORY AND DESIGN

Once the raw power supply is established via the battery pack, this energy must be harnessed appropriately to be delivered to the sensitive electronics on-board SeaLion. In the previous section, we specified the need for two voltage buses to deliver to the load electronics. These two buses are the 3.3V and 5V voltage rails. With the battery pack output of 12V, this voltage must be stepped down to 3.3V and 5V, respectively. This section discusses in detail how DC-DC voltage conversion, specifically step-down conversion, is performed and how the voltage converter design is implemented on SeaLion. Please note the phrases voltage regulator, step-down converter, and buck converter are used interchangeably in this section and throughout the thesis.

2.4.1 LINEAR VS. SWITCHING REGULATORS

One of the most important objectives in voltage conversion is energy efficiency. We need to be able to step-down the voltage without losing a significant amount of power in the process. Optimizing the efficiency of voltage converters is paramount in any power electronics application but deserves even more attention here in a satellite mission where power is such a precious commodity. This section discusses the difference between linear and switching voltage regulators and why switching regulators were ultimately chosen for SeaLion's EPS. Power efficiency will be the main performance factor compared between the two forms of regulation. A linear regulator is a form of voltage step-down converter where all the components of the converter are linear or only behave in their linear *active* regions. Linear components follow the property of superposition with respect to their input-output relationship of voltage and current. The simplest form of linear DC voltage regulation is via the voltage divider circuit. The voltage divider utilizes two resistance loads to split the input voltage to the designer's specification in the output. A typical voltage divider circuit is shown in Figure 14.

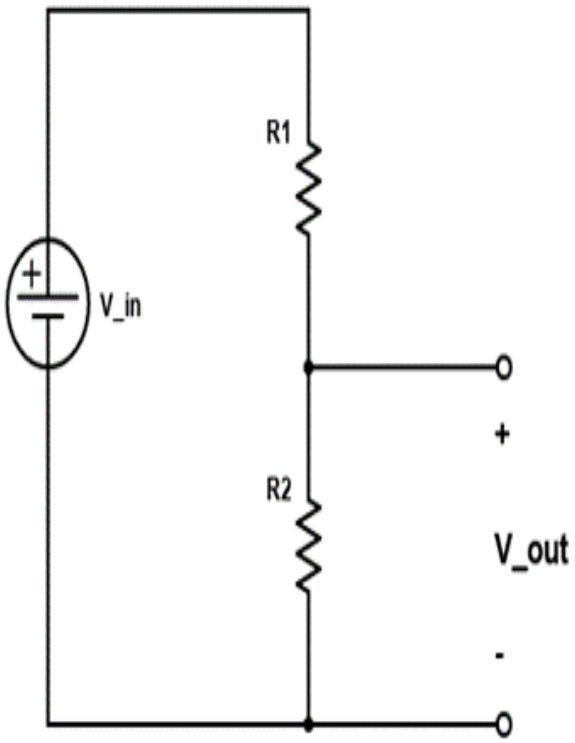

Fig. 14: Typical Voltage Divider Circuit

The output voltage becomes a function of the input voltage and R1 and R2 resistor values, given by (8).

$$V_{out} = V_{in} \frac{R_2}{R_1 + R_2} \tag{8}$$

The point of this voltage divider exercise is to demonstrate linear voltage regulators for DC-DC conversion are inferior to switching regulators in maximizing power efficiency. Although Figure 14 is the simplest version of a linear regulator, its behavior in terms of power efficiency from input to output mimics that of more advanced linear regulators. Using (9), we can calculate the efficiency of any power electronic circuit [26] to see how much power is lost through the dissipation of heated components, such as R1 in Figure 14.

$$\eta = \frac{P_{out}}{P_{out} + P_{loss}} \tag{9}$$

Plugging in SeaLion's starting voltage of 12V, efficiency was computed using (8) and

(9) in the voltage divider circuit for an increasing output load in R2. Figure 15 shows the results comparing power efficiency to output voltage for the voltage divider.

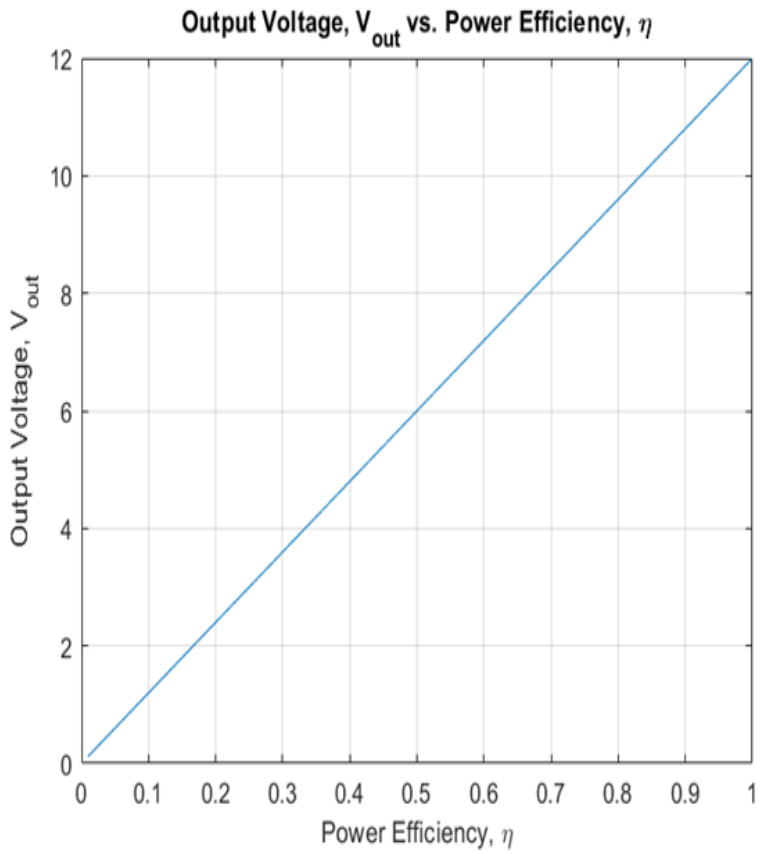

Fig. 15: Voltage Divider Output Voltage vs. Power Efficiency

The low-quality results here are exacerbated due to the simple nature of the voltage divider circuit but are important as this general relationship between output voltage and efficiency is consistent through any type of DC-DC voltage converter. The key takeaway is that the greater the decrease in voltage from input to output, the less efficient of the converter becomes. Larger in magnitude voltage step downs result in more power lost. This is also true in the more advanced linear regulators which are called low-dropout (LDO) regulators. LDO Regulators incorporate a transistor and an operational amplifier (op-amp) for feedback to correct the output voltage at the divider circuit. LDO regulators perform significantly more efficiently than a standard voltage divider circuit but are still not adequate for high efficiencies with an increased disparity in input to output voltage. There are higher efficiency LDO regulators available, but they often have smaller voltage

input ranges and cannot handle large voltage step-downs. Thus, switching mode voltage regulators are the solution for high efficiency applications. Switching regulators, known as Switched Mode Power Supplies (SMPS), are where transistors and diodes are operated as switches to ultimately control voltage level in the output. These switches are operated at a specific frequency that allows the circuit to control the desired average voltage in the output. This operation is called Pulse Width Modulation (PWM) where the width of the voltage is controlled by how long the switch is on and thus dictates the desired average DC voltage. The next section discusses how SMPS step-down voltage converters work and how their components were chosen for SeaLion.

2.4.2 SMPS BUCK CONVERSION

After establishing the need for a higher efficiency voltage conversion, we can now discuss in detail how this switched mode step down or buck converter is constructed for SeaLion's EPS. The basic structure of a SMPS DC-DC buck converter is shown in Figure 16. The switch is closed and opened at a certain frequency causing its output to be a periodic signal. The length of time for which the switch is closed or "on" is t_{on}, and the length of time for which the switch is open or "off" is t_{off}. The sum of these two lengths of time is the total time, T, of one cycle which is the period of the signal.

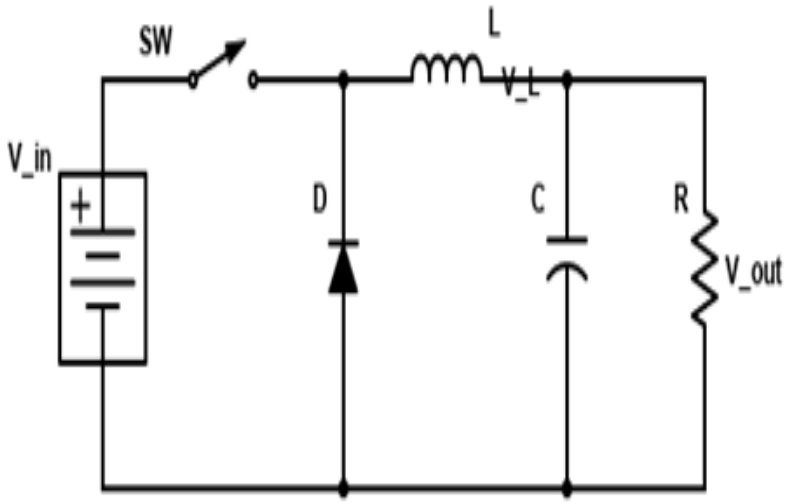

Fig. 16: DC-DC Buck Converter General Structure

The duty cycle, D, is the ratio of t_{on} to the total period T and dictates the width of pulse allowed to pass through the switch during one cycle. To derive the input-output relationship of the buck converter, we need to analyze the voltage at the inductor. In short, the inductor is the energy storage element of the circuit. It can hold and deliver energy to the load regardless of the on or off position of the switch. We start with KVL (3) to derive an equation for the inductor voltage for switch on and switch off states, shown in (10) and (11) respectively.

$$V_L = V_{in} - V_{out} \tag{10}$$

$$V_L = -V_{out} \tag{11}$$

To continue forward, the Volt-Second Balance law of an inductor [26] is introduced. This balance means the average voltage across an inductor for a periodic signal is zero, described mathematically by (12).

$$\frac{1}{T}\int_0^T V_L dt = 0 \tag{12}$$

Separating switch on time and switch off time to cover the whole periodic signal:

$$\frac{1}{T}\int_0^{DT} V_L dt + \frac{1}{T}\int_{DT}^T V_L dt = 0 \tag{13}$$

Then, plugging (10) and (11) into (13), the input-output relationship can be simplified to the result in (14).

$$V_{out} = DV_{in} \tag{14}$$

where D is the duty cycle described before. To derive the current being delivered to the load, we again go back to the inductor. The inductor current is a function of its voltage, described in (15).

$$i_L(t) = \frac{1}{L}\int_0^t V_L(t) dt \tag{15}$$

When the switch is on, we approximate the time derivative as a time difference of t_{on} or subsequently the multiplication of D and T. This results in the inductor current ripple equation (16), or the AC component of the inductor current [26].

$$\Delta i_L = \frac{1}{L}(V_{in} - V_{out})DT \tag{16}$$

Knowing the DC component of the inductor current will be its average current value, we can obtain the full equation (17) for the current going through the inductor.

$$i_L(t) = I_{L,avg} \pm \frac{\Delta i_L}{2} \tag{17}$$

To find the load current we can apply KCL (5) at the output node shown in Figure 17.

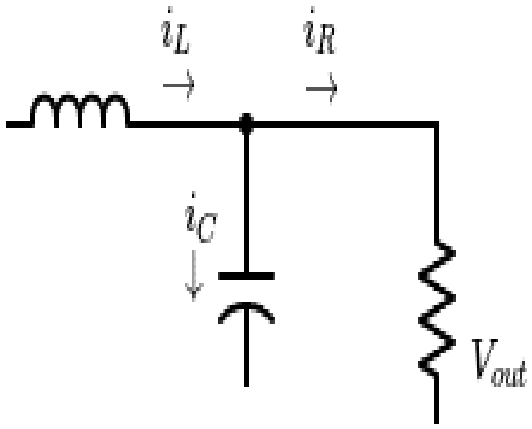

Fig. 17: Applying KCL at the Output Node of the Buck Converter

The capacitor ideally will only pass through the AC component of the entering current from the inductor. The DC component of the inductor current will be unable to pass through the capacitor as it will be seen as an open circuit. Therefore with the current ripple filtered out by the capacitor, only the average inductor current, $I_{L,avg}$, will be delivered to the load, meaning $I_{L,avg} = I_{out}$. With the buck converter governing equations established, we know have the means to analyze parameters and performance of commercially available buck converter integrated circuits (ICs).

2.4.3 VOLTAGE REGULATOR TRADE STUDY

A research-based trade study was conducted to select the voltage regulator for SeaLion's EPS. Parameters of COTS linear and switching regulators were compiled and analyzed to select the best fitting voltage regulator for the mission. Table 7 provides all COTS voltage

regulators compiled for comparison and analysis from popular electronics distributors and manufactures including *Digi-Key*, *Linear Technologies*, *Analog Devices*, *Maxim Integrated*, *Mouser*, and *Texas Instruments*.

TABLE 7: COTS Voltage Regulator Trade Study

Part No.	**Type**	V_{in} (V)	V_{out} (V)	**Max** I_{out}
LM2641	Switching	5.5 to 30	2.2 to 8	1000 mA
LM1572	Switching	8.5 to 16	2.42 to 5	830 mA
MAX639	Switching	4 to 11.5	5	150 mA
MAX750A	Switching	4 to 11	1.25 to 11	600 mA
LM2655	Switching	4 to 14	1.238 to 5	500 mA
MAX1761	Switching	4.5 to 20	1 to 5.5	600 mA
L7805-24	Linear	5 to 35	5 to 24	1.5 A
LM1084	Linear	Max 27, 25	3.3, 5, ADJ	5.0 A
LM1085	Linear	Max 18	3.3, 5, 12, ADJ	3.0 A
LM1117i	Linear	Max 20	1.25 to 13.8	800 mA
LM2941	Linear	6 to 26	5 to 20	1.0 A
L5973D	Switching	4 to 36	1.235 to 35	2.0 A
LM2576	Switching	1.23 to 37	3.3, 5, 12, 15, ADJ	3.0 A

We set criteria for selecting an appropriate step-down converter for SeaLion:

- Meet 12V input and 3.3V and 5V output requirements;
- Deliver up to 3.0 A to the output to meet electronic load requirement;
- High efficiency for varying current demand in the output (robust);
- Wide operating temperature range with at least $-40°$C on the minimum;
- Limited in complexity, i.e. Few components required, low monetary costs.

Ultimately, the LM2576 Switching step-down converter was chosen for SeaLion. The next section will discuss and analyze the parameters and associated component selections for the LM2576.

2.4.4 LM2576 VOLTAGE REGULATOR SETUP

The LM2576 buck converter is a simple yet sufficient DC voltage regulation solution for SeaLion. The converter meets all the set criteria and requirements stated previously. Table 8 lists some of these parameters from [27], [28] that satisfy the criteria.

TABLE 8: LM2576 Step-down Voltage Regulator Characteristics

Input/Output Voltage	V_{in} = 12V, V_{out}=3.3V, 5V
Max Current	3.0 A
Typical Efficiency	75-82% (for specified I/O voltage values)
Operating Temperature Range	-40 to 125°C
External Components Required	4

We will now consider the external components design for the LM2576. As shown in the SMPS Buck Conversion theory section, these components have an enormous impact on the performance of the buck converter. The component selections are based on the theory, datasheet recommendations [27], output ripple efficiency [29], and failure mode analysis [30].

Input Capacitance

The first component to consider from the manufacturer's [27] recommendation is a bypass capacitor at the input. The objective of this capacitor at the input of the buck converter is to reduce voltage and current transients, ripple, or noise at the input to deliver smooth DC voltage to the converter to step-down. AC transients and disturbances at the input could cause large unwanted oscillations in the voltage output [30] which could damage downstream electronics. The manufacturer recommends a $100\mu F$, 25V rated input capacitance for the LM2576 buck converter. A ceramic $100\mu F$ capacitor was chosen for the design.

Switching Diode Selection

The diode at the output of the switch (typically a transistor) is often called the switching diode or the catch diode. This diode is vital to the buck converter operation as it blocks current flow back to the source via a short when the switch is closed while simultaneously continuing to allow current to flow to the load and back to the inductor when the switch is open. The diode is selected based on its current rating, reverse voltage rating, and recovery time. A fast recovery time is needed to fulfill the switching requirement of the converter. This means the diode needs to change states quickly from blocking current to allowing current to flow with the opening and closing of the converter's switch. Schottky type diodes can switch fast while minimizing power loss due to the switching [26]. The LM2576 manufacturer recommends the Schottky type diode with a current rating equal to the maximum current output of the converter and a reverse voltage rating of at least 1.25 times the maximum input voltage [27]. With a maximum anticipated input voltage of 12V, the diode would need at least a 15V reverse voltage rating. The 1N5822 Schottky diode listed previously in Table 6 meets all of these requirements and was chosen for the buck converter circuit design.

Inductor Selection

The inductor, L, from Figures 16 and 17, must be chosen carefully for the buck converter to operate as intended. The inductor is the main storage element for current in the circuit, and without sufficient inductance the buck converter will not be able to deliver appropriate current to the load. An insufficient inductance can lead to the inductor becoming saturated, thus having its effective inductance slowly decrease with every switch interval [30]. The current in the inductor will rise and fall quicker and cause instability in the converter. The

current discharged from the inductor to the load can peak too high and trigger the LM2576 overcurrent latch or run too low and provide insufficient current to the load. Insufficient inductance in the converter can also lead to large peak-to-peak current ripple in the output [30]. This large current ripple can cause a slew of issues including additional power loss, lower power efficiency, and rises in temperature which can damage the inductor and surrounding components. The inductance value chosen is based on the LM2576 manufacturer data provided in their inductor value selection guide [27]. According to the data, an inductance value that can handle a maximum load current of 3.0 A and an input voltage of 12V for both the 3.3V and 5V fixed converters is $100\mu H$. With this inductance value established, the physical inductor must now be chosen for the design. The manufacturer states that the inductor current rating must be greater than the anticipated maximum peak current that will flow through the inductor [27]. They provide the equations (18) and (19) to verify the inductor qualifies for the anticipated voltage input-output relationship.

$$t_{on} = \frac{V_{out}}{V_{in}} \frac{1}{f_{osc}} \tag{18}$$

$$I_{p(max)} = I_{Load(max)} + \frac{(V_{in} - V_{out})t_{on}}{2L} \tag{19}$$

These two equations are just different ways of describing (16) and (17) already shown earlier, verifying the manufacturer's application recommendations with the buck converter theory. The term on the right-hand side of the sum operation in (19) is the output current ripple as calculated in (16). Using (16) and (19), we can calculate the anticipated current ripple in the inductor and the maximum anticipated current the inductor could see. Table 9 shows the results.

TABLE 9: Current Ripple in the Inductor

	3.3V Converter	**5V Converter**
Current Ripple	0.23 A	0.28 A
Maximum Inductor Current, $I_{p(max)}$	3.12 A	3.14 A
Percent Ripple of Max Load Current	7.67%	9.35%

Therefore, we need an inductor with a current rating of least 3.14 A but preferably higher to decrease the risk of inductor saturation. With this in mind, the COTS readily

available 4.0A rated *Abacron* AIRD-02-101 $100\mu H$ inductor was chosen for both 3.3V and 5V converter designs. The percent current ripple of the maximum load from Table 9 shows strong performance of the inductors in these buck converters as typical percentages are in the range of 10% to 40%. Not only will the higher inductance limit the current ripple, but it will also decrease conduction losses in the converter MOSFET switch [29]. A tradeoff, however, for the increased inductance, is the added Direct Current Resistance (DCR) rating of the inductor. The DCR rating increases with inductance, due to the added windings, and with inductor temperature and can cause significant power loss. This factor is considered in overall converter power efficiency. An additional disadvantage to a higher inductance value is the increased or *slow* transient response of the feedback control loop of the converter. This means the converter will take longer to adjust the voltage level when the converter load is changed. This can be combated with an appropriate output capacitor design.

Output Capacitor Selection

The output capacitor of the buck converter has two main functions: to filter out AC voltage transients and ripple from going to the DC load and to provide stable operation of the feedback control loop system of the converter. The manufacturer recommends that the voltage ripple in the output be approximately 1% of the output voltage to maintain stable feedback operation and acceptable voltage delivery to the load [27]. To obtain the voltage ripple across the capacitor we start with the capacitor's voltage-current relationship.

$$i_c = C\frac{dV}{dt} \tag{20}$$

$$V_c(t) - V_c(0) = \frac{1}{C}\int_0^t i_c(t)dt \tag{21}$$

Since only the inductor ripple current, the AC component of the current, will pass through the capacitor, we can deduce the integral in (21) to the triangular area of the inductor ripple current, which leads to (22) [31].

$$\Delta V_c = \frac{T}{8C}\Delta i_L \tag{22}$$

From (22), it can easily be seen that greater capacitance directly reduces voltage ripple across the capacitor. However, the disadvantage to a higher capacitance is an increase in capacitor Equivalent Series Resistance (ESR). A capacitor based on its material and physical construction, has some inherent series resistance called ESR, and this must be accounted for in the buck converter design. The ESR can amplify an unwanted voltage spike in the output

in the transient response [29]. This spike can slow down the transient response or even cause damage to sensitive electronics in the load. The ESR will draw additional current to the capacitor and in turn increase the voltage ripple across it. This additional voltage term is introduced in (23).

$$\Delta V_c = \frac{T}{8C}\Delta i_L + \Delta i_L \times ESR \tag{23}$$

Ideally, the ESR term for the capacitor is small and does not add significant voltage ripple or the output capacitor would not be worth installing for the converter. The capacitor material and size dictate its ESR value. For each bus we can calculate the capacitance required using (23) to satisfy the 1% ripple of the total output voltage recommendation. Continuing with the manufacturer's documentation, for the stable loop operation, the capacitor must satisfy a minimum requirement of (24).

$$C_{out} \geq \frac{V_{in}}{V_{out}} \times L(\mu H) \tag{24}$$

This results in approximately $483.6\mu F$ and $319.2\mu F$ for the 3.3V and 5V converters, respectively. Even with this minimum requirement, a capacitance value between $680\mu F$ and $2000\mu F$ is still recommended for improved performance in voltage ripple and the transient response of the converter. The capacitor material recommended is aluminum electrolytic; however, aluminum electrolytic capacitors should be avoided. The reason for this will be discussed in the next section. Two COTS readily available–*Vishay* tantalum capacitors of $470\mu F$–were added together in parallel at each converter output to achieve a $940\mu F$ total capacitance. These tantalum capacitors boast an "ultra-low" ESR of $30m\Omega$ [32]. With this capacitance and ESR, (23) is used to achieve the voltage ripple and percent ripple performance markers in Table 10. The percent ripple of the total output voltage is significantly under the suggested 1% for each converter.

TABLE 10: Voltage Ripple at the Output Capacitor

	3.3V Converter	**5V Converter**
Voltage Ripple	14.4 mV	17.5 mV
Percent Ripple of Voltage Output	0.44%	0.35%

A General Note on Capacitors

The capacitor selections for a DC-DC buck converter have immense impact on its performance and efficiency, but capacitors are also used in many components in the electrical design and payload of SeaLion. Therefore, the material used in these capacitors must be carefully discussed and reviewed to ensure they fit these applications and that they operate properly in the space environment. Three common, readily available capacitor materials: aluminum electrolytic, ceramic, and tantalum will be discussed. This section is meant to explain why aluminum electrolytic capacitors are excluded from the converter, opposing the LM2576 manufacturer's recommendation, and other electrical designs of SeaLion.

For DC-DC voltage converters, [29] and [33] give in-depth treatments of the most suitable materials for capacitors in the converter setup. Capacitors are analyzed based on material, physical size, ESR, and monetary cost in [29]. The physical size characteristic of capacitors is referred to as volumetric capacitance, meaning how much capacitance is available for the pure volume that the capacitor consumes. This is obviously important in a CubeSat mission where onboard volume is severely constrained. The aluminum electrolytic capacitor performs the worst in this category when compared to ceramic and tantalum type capacitors [29]. The ESR, as mentioned before, is the inherent series resistance of the capacitor. Ideally, we would treat capacitors as purely reactive components, but this does not hold true in their physical implementation. The objective is to have the smallest ESR value to reduce power losses in the capacitor since ideally it is not meant to consume power. Aluminum electrolytic capacitors have greater ESR values in comparison to ceramic and tantalum making them again a less suitable choice of material. The best performance in terms of ESR is ceramic capacitors, as they generally have at least an order of magnitude less ESR than tantalum capacitors [29]. Ceramic capacitors seem to be the optimal fit for most applications but are limited in capacitance as they are generally not readily available at capacitances above $100\mu F$. This poses a problem for the buck converter output capacitor, as shown in (24), where the bare minimum capacitance required is much greater. To meet the capacitance requirement in the output, tantalum capacitors are chosen for the design. The harsh environment of space must also be considered when choosing capacitors for a satellite mission. Radiation experienced in orbit can cause dieletric breakdown of the capacitor and degrade it much faster than its rated lifetime [34]. This can cause the capacitor to "short" rendering its capacitance negligible. From [34] and the Space Material Handbook NASA SP-3025 [35], ceramic material is the most resistant to radiation while electrolytic material is susceptible to radiation degradation and is considered *poor* in radiation stability. For this

additional reason, ceramic capacitors are used exclusively in SeaLion except at the output of the buck converters where a greater capacitance is required.

2.5 OVERVOLTAGE AND OVERCURRENT PROTECTION

From the previous COTS review of GOMSpace and AAC Clyde EPS, it is apparent protection circuitry is utilized to prevent damage and failure of the EPS and load electronics. The available literature and accessible EPS design reviews for small satellites all incorporate some form of voltage or current protections. See [36], [37], [38], [39], and [40], for variety in protection circuitry implementation. The obvious objective of this circuitry is to increase the *reliability* of the EPS and prevent *failure* of the payload electronics. Failure and reliability of systems are difficult to measure but for the purposes of this section, EPS success can be simplified to successful voltage and current delivery. Voltage and current delivery must be sufficient but not too great as to overcharge and destroy the payload electronics. For a full failure analysis of the Mission SeaLion including the EPS components, see [41]. For space missions, the main environmental concern for the electronics is the radiation effects in orbit. Radiation can cause bit flips or errors in logic lines and even catastrophic failure in onboard transistors by short circuiting [37]. See [37] for details on specific electronic design event failures caused by radiation effects.

The protection circuitry chosen for SeaLion is meant to provide overcurrent, overvoltage, and undervoltage protection. These values are driven by the system requirements and anticipated electrical loads of the onboard electronics and sensors. The protection circuitry must be able to locally measure voltage and current and take action depending on designated threshold values. Two main design factors were considered: simplicity of design (i.e. auto-reset, low number of components) and customizable current threshold. The LTC4361-2 IC [42] was ultimately chosen to satisfy the protection circuitry requirement, following [38] in their overcurrent IC choice. In [37], [43], hardware solutions are preferred in overcurrent protection to reduce complexity and increase efficiency. Involving the software via OBC or a microcontroller to measure, detect, and drive a shutdown and reset when a fault occurs was beyond the scope of design and introduces many additional control variables and points of failure. There are two variations of the LTC4361 IC; the LTC4361-1 and LTC4361-2. The -1 model engages an internal latch-up when an overcurrent fault occurs. This latch must be manually reset by cycling an appropriate voltage level through separate pin on the IC. The -2 model automatically resets from an overcurrent fault detection after a 130 ms start-up delay [42]. The -2 model was chosen to reduce complexity of the circuitry to

make it completely independent and autonomous post-installation. Both models, however, will conduct an auto-retry after an overvoltage fault. Table 11 shows the parameters of the LTC4361-2 IC implemented in a KiCAD schematic in Figure 18.

TABLE 11: LTC4361-2 Fault Thresholds

Overcurrent Fault Threshold	3.0A
Overvoltage Fault Threshold	5.8V
Undervoltage Fault Threshold	2.1V

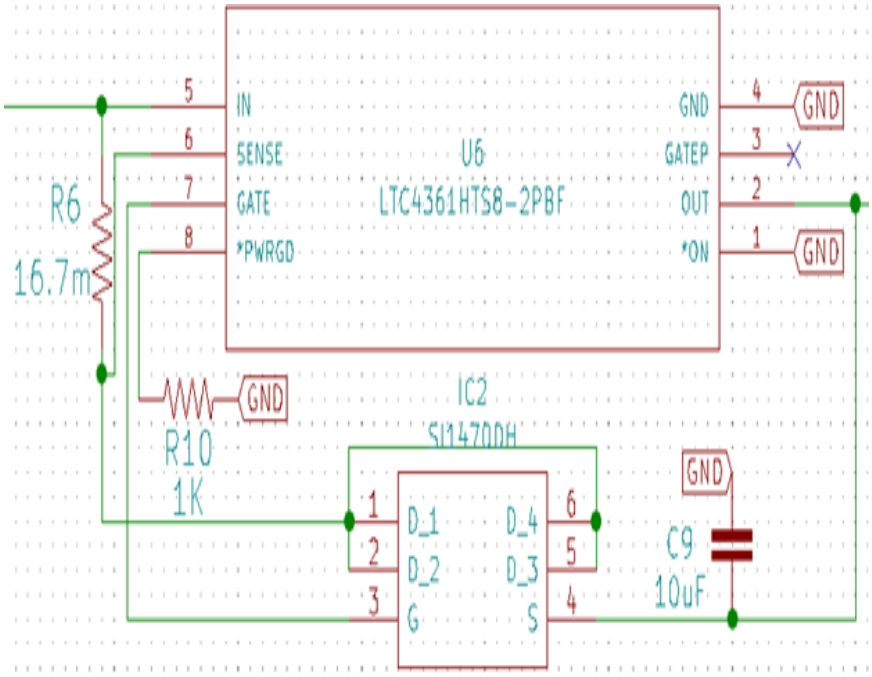

Fig. 18: KiCAD Schematic Implementation of LTC4361-2 Overcurrent IC

The voltage is measured across the sense resistor, R6 in Figure 18, to detect an overcurrent fault. This resistance value is chosen to set the overcurrent threshold at 3.0 A. Although the importance of the protection circuitry was stressed to prevent PCB short circuits from damaging the electronics, it is implemented in SeaLion as a redundancy. The LM2576 buck converter has also 3.0 A latch current limiter and thermal shutdown ability if excessive current is being drawn due to a short [27]. The converter output feeds the LTC4361-2 IC and therefore prevents this IC from being the single point of failure in the protection system.

CHAPTER 3

ANALYSIS OF SEALION ELECTRICAL POWER SYSTEM

3.1 VOLTAGE REGULATOR SIMULATION AND ANALYSIS

A computer simulation and analysis of the LM2576 buck converters based on the selected components was performed to verify the performance of the voltage regulation and available current delivered to the load. The circuits were constructed and simulated in *OrCAD* PSpice software. Figure 19 shows the two LM2576 converter circuits and associated electrical components with performance-based designed parameters derived in the previous section. Note the inductors' DCR and capacitors' ESR values are added to the circuits to make the simulation as realistic as possible by modeling what will be encountered in the actual application.

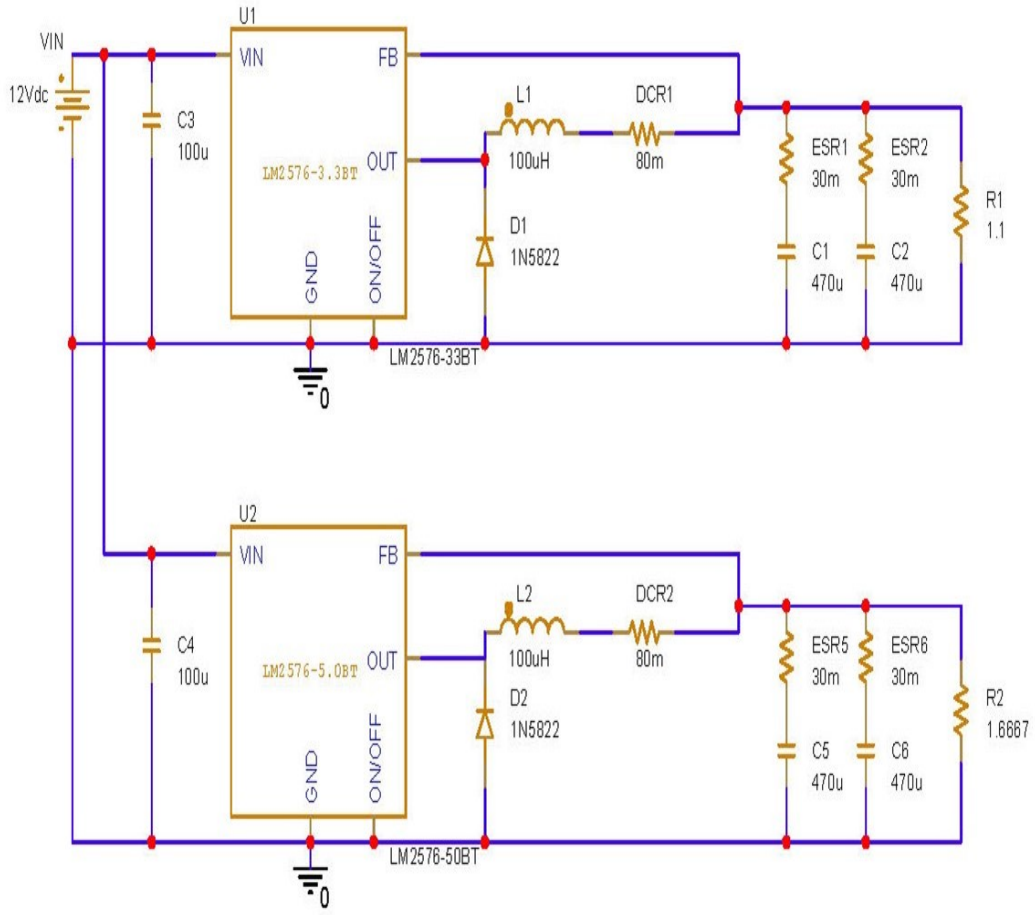

Fig. 19: PSpice LM2576 3.3V and 5V Buck Converter Circuits

From Figure 19, we can see the circuit simulation setup mimics that of the design of the EPS. A raw battery voltage of 12V is applied to two LM2576 buck converters. As expected, the circuits are set up so that the LM2576-3.3 IC steps the voltage down to 3.3V, and the LM2576-5 IC steps down the voltage to 5V. R1 and R2 are the load resistors, and they mimic the anticipated loads for each bus. Their values were chosen to draw a 3.0 A load current at each resistor. This level of current is not expected to be seen by the converter based on the anticipated electronic load of SeaLion, but placing the maximum load on the converter is best for simulation to ensure it can perform at a high level. Figures 20 and 21 are the time domain responses of 3.3V and 5V converters, respectively. The green plot indicates the output voltage, V_{out}, and the red plot indicates the output current, I_{out}.

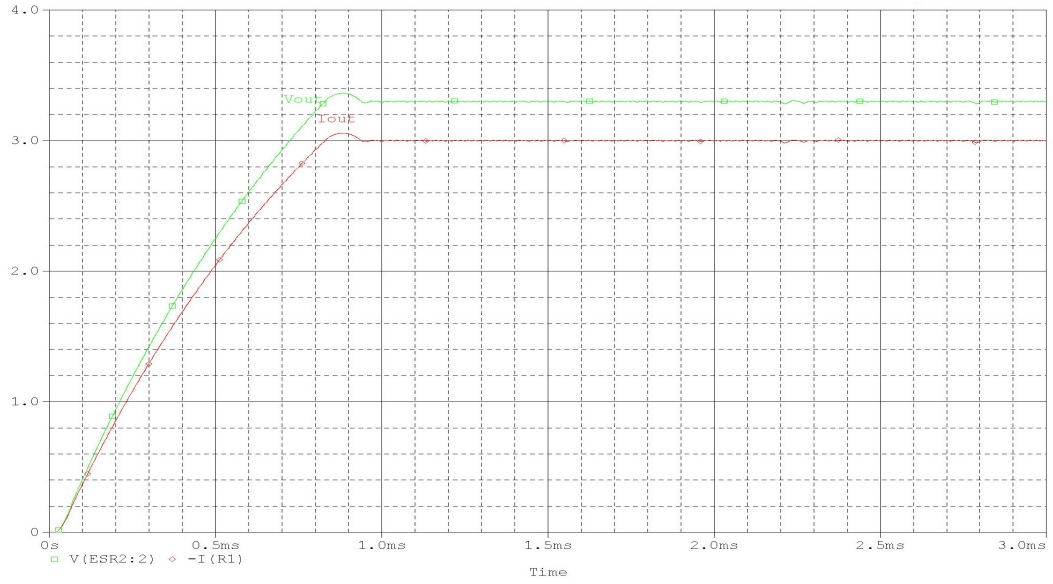

Fig. 20: PSpice Simulation Results of Time Domain Response for Output Voltage and Current of the LM2576 3.3V Buck Converter

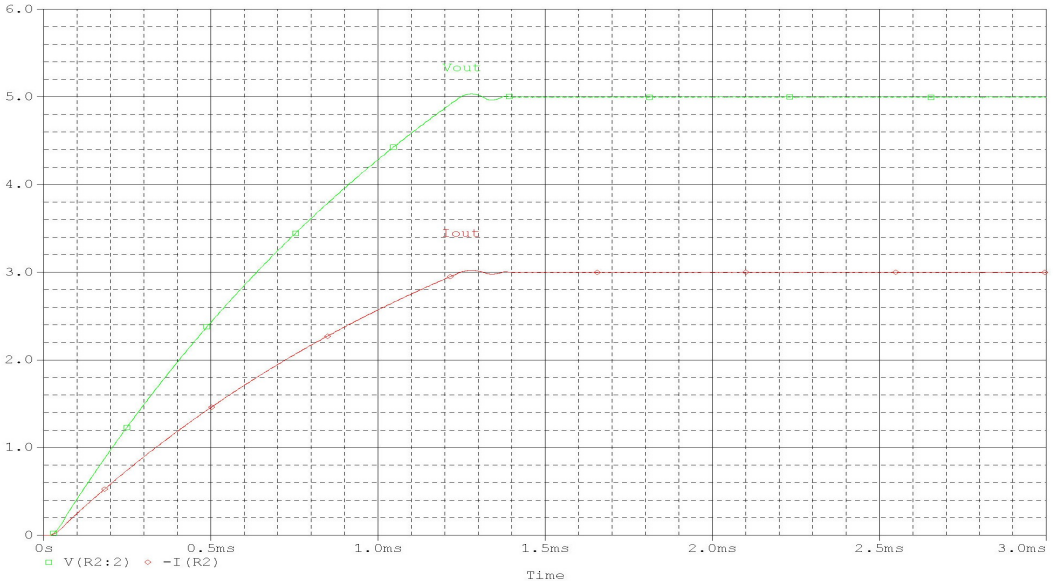

Fig. 21: PSpice Simulation Results of Time Domain Response for Output Voltage and Current of the LM2576 5V Buck Converter

We can see from Figures 20 and 21 that both converters behaved as expected. After the initial transient response of the converter, the respective intended voltage outputs of 3.3V

and 5V were reached and remained there in the steady state. Of note is the difference in *percent overshoot* between the two converters. Percent Overshoot (%OS) is a control system parameter that identifies proportionally how much the time response waveform rises above the final steady state value in its initially transient response [44]. The %OS is found by

$$\%OS = \frac{c_{max} - c_{final}}{c_{max}} \times 100\% \tag{25}$$

To evaluate the performance further, we extracted the output ripple current and output ripple voltage data from the simulation. Since these values are highly dependent on the inductor and capacitor selection, the data will affirm our decisions in their selection and verify their placement in SeaLion's EPS design. From the simulation, both buck converters performed well in voltage and current ripple, verifying the design choices. Figures 22 and 23 show the output ripple data for the 3.3V converter simulation while Figures 24 and 25 show the output ripple data for the 5V converter simulation.

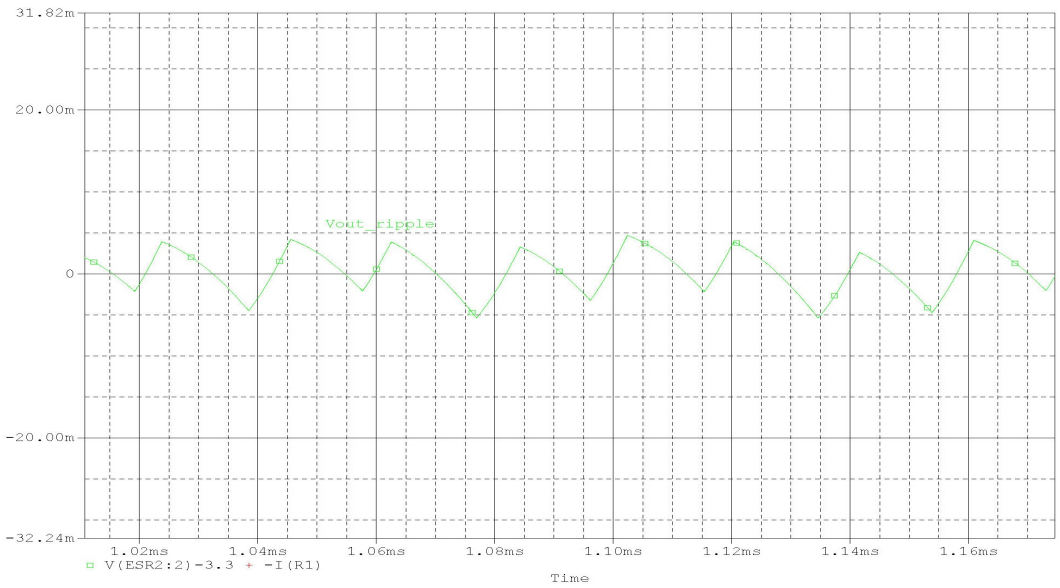

Fig. 22: Output Voltage Ripple Data from the LM2576 3.3V Buck Converter PSpice Simulation

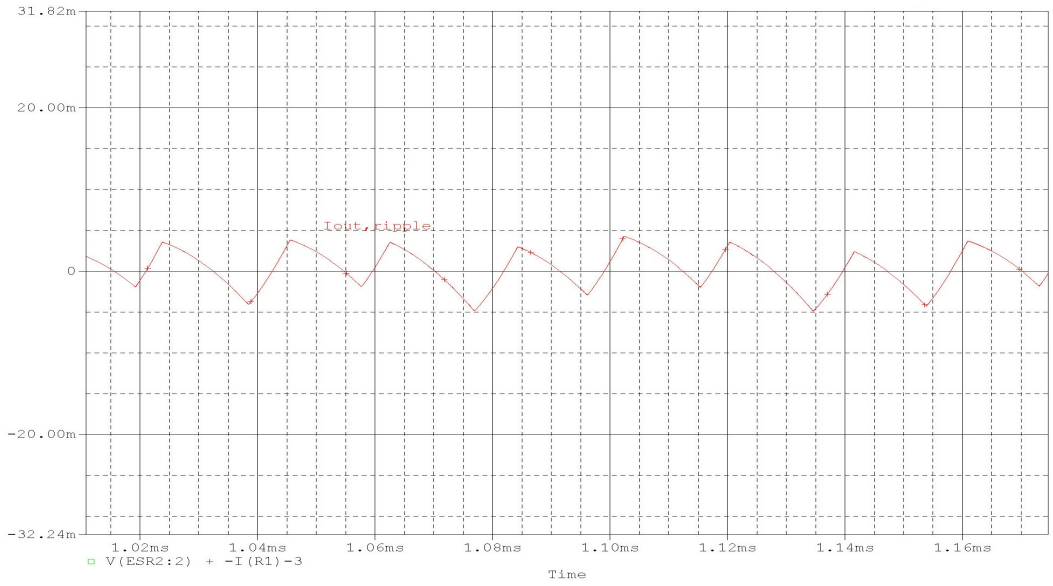

Fig. 23: Output Current Ripple Data from the LM2576 3.3V Buck Converter PSpice Simulation

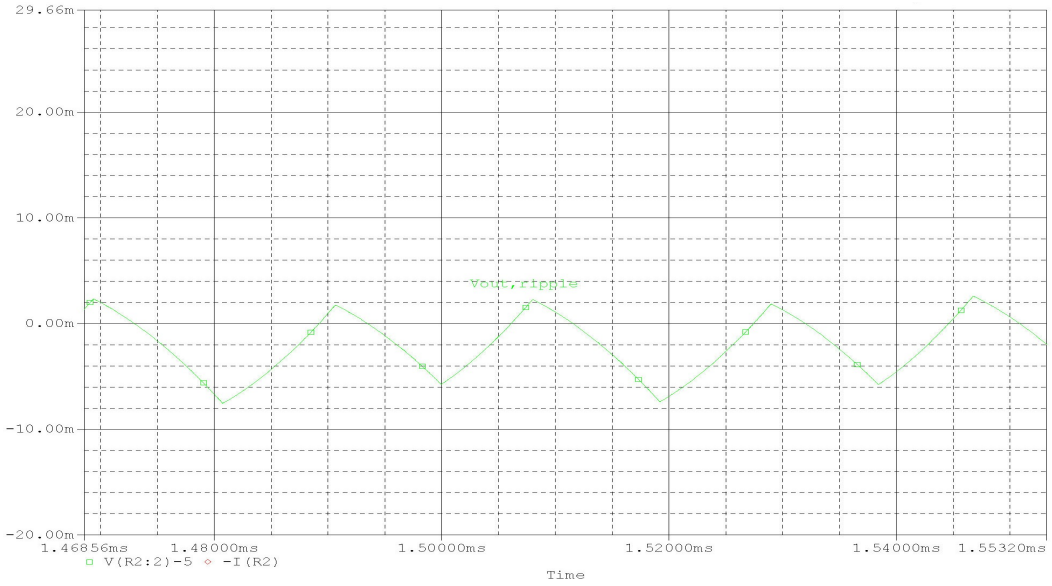

Fig. 24: Output Voltage Ripple Data from the LM2576 5V Buck Converter PSpice Simulation

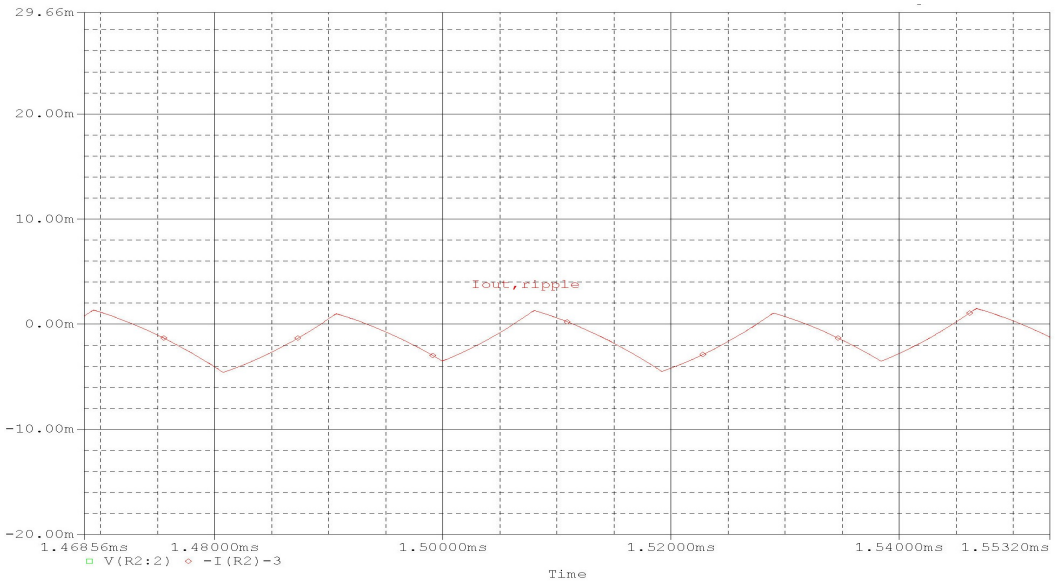

Fig. 25: Output Current Ripple Data from the LM2576 5V Buck Converter PSpice Simulation

Extracting the data from the ripple plots, we compiled the peak-to-peak voltage and current ripple values as well as %OS for each converter in Table 12.

Comparing Table 12 with Tables 9 and 10 from the original design, we show that the LM2576 performed as expected or better in the PSpice Simulation, having approximately the same or lower values in ripple magnitude and percent ripple for voltage and current for both voltage buses. The percent overshoot is exceptionally low for a second order system [44] and ensures the converter will succeed in handling load changes without the output voltage exceeding the converters' operation range. As expected, the 3.3V converter was less efficient in voltage and output current ripple than the 5V converter with the same input voltage of 12V. The 3.3V converter simulation also had 12 mA more current ripple in the inductor than in the original design calculations, meaning the inductor DCR and capacitors' ESR values had more impact on the 3.3V converter. This result supports our original hypothesis that for a general DC-DC step-down converter, a greater magnitude disparity between V_{in} and V_{out} will result in less power conversion efficiency. This is also supported by the LM2576 datasheet [28] which lists 75% expected efficiency for the fixed 3.3V converter and 82% expected efficiency for the fixed 5V converter. Now that the simulation and analysis is complete, the DC-DC voltage regulator design is verified, the EPS design can be reviewed.

TABLE 12: PSpice Simulation Ripple Results

	3.3V Converter	**5V Converter**
Voltage Ripple	9.2 mV	9.6 mV
Percent Ripple of Voltage Output	0.27%	0.19%
Output Current Ripple	8.4 mA	5.8 mA
Inductor Current Ripple	0.242 A	0.262 A
Percent Ripple of Current Output	8.07%	8.73%
Percent Overshoot	1.92%	0.67%

3.2 DESIGN OVERVIEW

With the major components for the EPS established, the EPS PCB schematic was designed. The EPS board takes in the battery pack power output, steps-down its raw 12V voltage to 3.3V and 5V buses, and delivers this to SeaLion's payload and electronics via a PC-104 interface pin block. Two additional EPS features were included to compare with the COTS modules as discussed earlier. The first is the ability to monitor voltage and current at different points in the EPS. This data will enable the OBC to track total power consumed for the mission and ensure bus voltages are at appropriate levels for the load electronics. The LTC2944 Battery Fuel Gauge IC is placed to measure the raw battery output and will provide battery voltage and total current draw data to the OBC [45]. Two total LTC2990 ICs [46], one for each voltage bus, are placed after the voltage converters and overcurrent protectors to monitor the voltage and current on each bus that is going to the load. The LTC2944 and the LTC2990 ICs both will transmit data to the OBC via the I2C communication standard [46]. The second feature is the Remove Before Flight (RBF) switches and connection for the deployment switch. The RBF and deployment switches are required by launch providers (such as *NanoRacks* [47]) to ensure source power does not reach the load and activate any electronics before or during launch. The EPS schematic designed using KiCAD PCB design software is shown below in Figure 26.

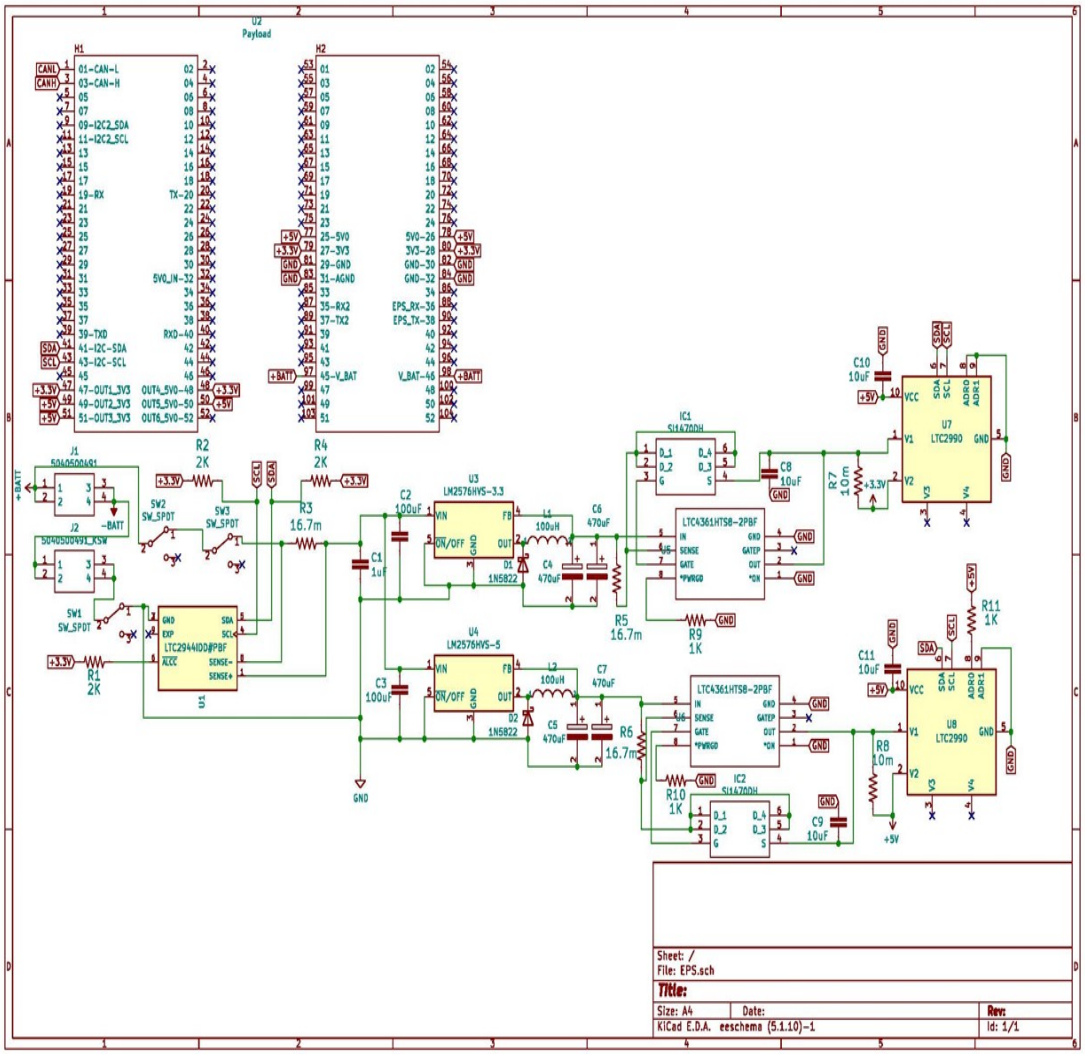

Fig. 26: Full EPS Design via KiCAD PCB Software Schematic

3.3 POWER BUDGET ANALYSIS

A few estimated requirements had to be established to design the EPS as shown in the previous section. EPS requirements like the specific voltage buses (3.3V, 5V) needed and estimated power consumed during the mission (100-150 Wh) had to be proposed early on to design the EPS. Now that the EPS design is finalized, a true power budget can be computed utilizing all of the components selected here for the EPS, for SeaLion's other general functions and operations, and importantly the science payloads. A power budget

analysis is critical for a space mission to verify there is enough electrical power to operate as intended for the mission duration and perform all the required mission objectives. The first set of data introduced in Table 13 lists every significant component currently (at the time of this writing) selected that requires and consumes electrical power to operate.

The total power consumed for one hour, if all these components were fully active, is approximately 9.09 W. To preserve and extend the available power for the mission, components are duty cycled. This means that components will be set off or inactive when they are not needed at the specific time for mission operations. Working with the flight software and mission operations team members of SeaLion, I was able to rework the power budget to fit SeaLion's concept of operations' mission modes described by the CDR. Each designated mission mode needs specific components active while others can remain inactive and not consume as much, if any, electrical power. Table 14 shows anticipated total power consumption for each mission mode based on the active electronics for that mode.

We can estimate the total power consumed daily while in orbit by evaluating each mission mode and its expected active duration. Based on the concept of operations for the mission, Table 15 estimates the active time duration for each mission mode.

With this data, we can calculate the expected power consumption at any point in time over the mission duration. The total power consumed by SeaLion over varying points in time of the mission is shown in Table 16.

To verify the anticipated mission duration, we need to calculate the efficiency of the power being delivered from the battery pack to the load. We know from before that the voltage regulators for each voltage bus are not ideal, and they consume power to operate. This means they will contribute to power loss when converting the raw battery voltage to the 3.3V and 5V voltage buses. From the LM2576 Voltage Regulator Datasheet [28], the expected efficiency of the 3.3V converter is 75% and the 5V converter is 82%. Taking this worst case 75% efficiency value, we can compute the estimated available power for the mission. Table 17 shows the estimated total mission power found by computing the product of the battery energy capacity and the worst case voltage regulator efficiency. From Tables 16 and 17, we can determine that there will be enough power available for SeaLion to operate fully as intended for at least 7 days.

TABLE 13: Mission SeaLion Total Power Budget

Module	**Component**	**Quantity**	**Current (mA)**	**Voltage (V)**	**Power (mW)**
COMMS 1	UHF Tx	1	800	3.3	2640
COMMS 1	UHF Rx	1	55	3.3	181.5
COMMS 2	S-Band Tx	1	725	5	3625
COMMS 2	S-Band Rx	1	112	5	560
OBC	A3200	1	45	3.3	148.5
OBC	MPU-3300	1	10	3.3	33
OBC	HMC5843	1	0.28	3.3	0.924
AODS	Sun Sensor	6	0.1	3.3	1.98
AODS	ADIS16400 IMU	1	70	5	350
AODS	GPS	1	272.73	3.3	900.009
EPS	LTC2944I	1	0.85	12	10.2
EPS	LTC2990	2	1.1	5	11
EPS	LTC4361-2 (3.3V)	1	0.22	3.3	0.726
EPS	LTC4361-2 (5V)	1	0.22	5	1.1
CGA Payload	Impedance Probe	1	x	x	0.1966
CGA Payload	Ms_S	1	x	x	0.25
DeCS	DeCS Encoder	1	120	5	600
DeCS	Strain Gauge	4	1.5	5	30
Total power (mW)					9094.386
Total power (W)					9.094386

TABLE 14: Operating Mission Modes Power Budget

	Max Power Per Operating Mode				
Mission Mode	**Safehold**	**Comms**	**Mission1**	**Mission2**	**Mission3**
Total power (W)	1.329	7.452	2.829	2.829	3.093

TABLE 15: Mode of Operation Active Time per 24 Hours

Mode	**Time Active Per 24 Hours**
Safe Hold	22 hrs 30 mins
Comms	30 Min
Mission 1	20 Min
Mission 2	20 Min
Mission 3	20 Min

TABLE 16: Total Power Consumed Per Time Interval

Total Duration	1 Hour	1 Day	3 Days	5 Days	7 Days	8 Days
Power Consumed (W)	1.52	36.6	109.7	182.8	255.9	292.4

TABLE 17: Estimated Available Power Calculation

Battery Energy Capacity (Wh)	384
Worst Case Voltage Regulator Efficiency	0.75
Estimated Available Power (Wh)	**288**

CHAPTER 4

DESIGNING THE COMMUNICATION SYSTEM FOR THE SEALION MISSION

The existing satellite communication infrastructure of the Virginia CubeSat Constellation (VCC) has greatly reduced the complexity of SeaLion's communication design. Old Dominion University's existing operational ground station [48], enables UHF communication with LEO spacecraft and has already been tested and prepared with a previous ODU CubeSat mission in mind. See [14] for communications design and orbital analysis of ODU's most recent 2019 mission, *VCC Aeternitas*. With the Virginia Ground Station Network (VGSN) already established in [49], ODU's ground station in [48], and a CubeSat mission analysis in [14], this section will focus solely on SeaLion's communications components and link budget utilizing orbital analysis contributed from SeaLion operations team members.

4.1 FREQUENCY, HARDWARE, AND GROUND STATIONS

The operating frequencies of the intended ground stations drove the design choices for SeaLion's onboard radios and radiating antennas. From the primary mission objectives, SeaLion shall have two communication links established in the UHF and S-Band frequency ranges. The ODU ground station is optimally designed to operate at 401 MHz, leading SeaLion to have a UHF operating center frequency at 401.08 MHz and in keeping with the same infrastructure as *VCC Aeternitas* [14]. The UHF radio will operate at half-duplex, meaning it will transmit and receive at different time intervals. The chosen radio hardware is the GOMSpace NanoCom AX100 UHF Transceiver shown in Figure 27. Here are the key factors behind design decision [50]:

- Simple interfacing with chosen GOMSpace OBC,
- GMSK modulation and AX.25 Protocol [51] packet formation capable,
- 3.3V Power Supply matching EPS capability,
- Acceptable data rate capability,
- Sufficient Transmit/Receive Power.

Fig. 27: GOMSpace NanoCom AX100 UHF Transceiver

The second communication link in the S-Band frequency needs to be established to communicate with the Mobile CubeSat Command and Communications (MC3) network and specifically the ground station located at USCGA in New London, CT. The MC3 network is operated by the Naval Postgraduate School and is meant for ground to space communications for use by the Department of Defense (DoD) and its partners for research and development [52]. In the partnership between ODU and USCGA, the MC3 network became accessible for communications and a novel objective for SeaLion. To coincide with the operating frequency range for the USCGA MC3 ground station, an uplink center frequency of 2037.5 MHz and downlink frequency of 2232.5 MHz were assigned to SeaLion. Staying consistent with the hardware interfacing and support for the UHF AX100, the GOMSpace NanoCom AX2150 S-Band Transceiver [53], shown in Figure 28, was chosen for use onboard SeaLion. At the time of this writing, ODU and Virginia Tech are in the process of applying for a joint experimental license from the Federal Communications Commission (FCC) to obtain permission to operate at these respective UHF and S-Band frequencies.

Fig. 28: GOMSpace NanoCom AX2150 S-Band Transceiver

4.2 GMSK MODULATION

Gaussian Minimum Shift Keying (GMSK) is the digital modulation scheme used for UHF and S-Band communications onboard SeaLion. GMSK is a type of Minimum Shift Keying (MSK) which is a subset of Frequency Shift Keying. FSK utilizes two or more orthogonal signals at differing frequencies to transmit messages [54]. MSK enhances FSK by spacing the orthogonal signals specifically to minimize the bandwidth, making the two signals *coherently* orthogonal. To derive MSK, we start with a Continuing Phase FSK (CPFSK) signal in (26)

$$s(t) = \sqrt{\frac{2E_b}{T_b}} \cos[2\pi f_c t + \theta(t)] \tag{26}$$

where E_b is the energy per bit, T_b is the bit duration, and f_c is the center frequency. The signal, $s(t)$, is always continuous since the phase $\theta(t)$ is continuous [55]. The phase of the CPFSK signal is given by

$$\theta(t) = \theta(0) \pm (\frac{\pi h}{T_b})t \tag{27}$$

where h is the deviation ratio. The relationship between orthogonal frequencies can be deduced from (27) to (28):

$$h = T_b(f_1 - f_2). \tag{28}$$

When $h = \frac{1}{2}$, CPFSK becomes MSK since the minimum spacing in frequency, $\Delta f = \frac{1}{2}T_b$, between the signals is achieved while still staying orthogonal to one another [54]. MSK is advantageous and used in digital communications since it has a narrow-bandwidth occupancy, a constant modulated signal envelope, can be coherently detected [55]. However, its power spectral density can still be optimized to allow for additional users in the band while maintaining orthogonality between the message signals. This is performed by introducing a Gaussian low-pass pulse-shaping filter before the MSK modulation of the signals. Gaussian pulse-shaping filters are common in signal and image processing to optimize the frequency response of a system by narrowing the pulse energy around a tighter, more closely knit band of frequency. While still satisfying $h = \frac{1}{2}$ in (27) and (28), the frequency response now has a more narrow bandwidth with better performance in the intended stopband [55]. The new impulse response should also still have a low overshoot to avoid major deviations in instantaneous frequency to preserve the continuous-phase nature of the CPFSK base [55]. With the Gaussian pre-pulse-shape filtering, MSK now becomes GMSK. The frequency response and impulse response of GMSK are given by (29) and (30), respectively.

$$H(f) = \exp[\frac{-\ln(2)}{2}(\frac{f}{W})^2] \tag{29}$$

$$h(t) = \sqrt{\frac{2\pi}{\ln(2)}}W \exp(-\frac{2\pi^2}{\ln(2)}W^2t^2) \tag{30}$$

With the frequency and impulse responses both in forms of Gaussian functions, pulse shape is designed based on the time-bandwidth product, WT_b. The greater the time-bandwidth product the narrower the pulse in bandwidth. One additional value is required to analyze a GMSK communication system, and this is the probability of bit error, P_e, given in (30).

$$P_e = Q(\sqrt{\alpha\frac{E_b}{N_0}}) \tag{31}$$

where N_0 is the noise spectral density of the signal. The parameter α is directly related to the time-bandwidth product and inversely proportional to it. This means that a lower probability of bit error can be achieved with a greater value in WT_b.

GMSK has become increasingly popular for use in CubeSat communications. [56] analyzed active CubeSAT missions in 2014 and found that 24% of all active CubeSats at the time were employing a GMSK modulation scheme. The VGSN was designed with this in

mind, and GMSK has become the preferred modulation scheme for CubeSat to ground communications given data rate and Signal to Noise Ratio (SNR) requirements along with its proven reliability and flight heritage in the packet radio community [56].

4.3 ANTENNA DESIGN

SeaLion requires a separate antenna system for both the UHF and S-Band communication links. The main objective of the antenna designs is to achieve an omni-directional, or as close to omni-directional, radiation pattern as possible for each frequency band. An antenna with an omni-directional radiating pattern gives SeaLion the best chance of success to communicate effectively since SeaLion will not have attitude control capability. Without the ability to point toward Earth and, thus, the ground stations, unidirectional antennas can significantly decrease the probability of establishing a radio communication link from CubeSat to ground and vice versa. For the UHF antenna design, the crossed or turnstile half-wavelength dipole antenna was designed to achieve an omni-directional radiation pattern at the desired 401.08 MHz center frequency. The CubeSat Antenna Design Guidebook says the turnstile antenna is considered a Low Gain Antenna (LGA) that is beneficial for LEO UHF or S-band communications, and its omni-directionality enables the satellite to continuously communicate with the ground station without precising pointing or constantly rotating [57]. Providing antenna theory to support the design, we start with finding the wavelength of the antenna.

$$\lambda = \frac{c}{f} \tag{32}$$

where f is the radiating frequency and c is the speed of light. The crossed dipole antenna consists of two radiating half-wavelength dipole elements or four radiating quarter-length wavelength elements with a shared feed point at the intersection [58]. Each of the four elements of the crossed dipole should be $\frac{\lambda}{4} = 187mm$ in length; however, this is not taking the input impedance of the dipole into consideration. The antenna literature [58] addresses this issue specifically. [58] states the final input impedance of a half-wavelength dipole is approximately $73 + j42.2\Omega$. In order to maximize power transfer and radiation efficiency, the reactance must be reduced to as near zero as possible. The exact length where the reactance is zero is dependent on the element diameter and the input gap. With these characteristics in mind, the exact length is notably "just short" of the half-wavelength mark. [58] recommends starting element at 95% of its half-wavelength,

$$.95 \times \frac{\lambda}{2} = 355.3mm, \tag{33}$$

and then dividing the two half-wavelength elements into four quarter wavelength elements

$$.95 \times \frac{\lambda}{4} = 177.6mm. \tag{34}$$

Achieving a near zero reactance by cutting the elements to the appropriate electrical length avoids the need for additional impedance matching circuitry. With (33) and (34), we now have a baseline of what the element lengths should approximately be to minimize radiating power loss due to an impedance mismatch.

In addition to support from the theory, the crossed dipole for SeaLion was designed based on a proven model constructed and designed previously for the VCC Aeternitas ODU CubeSat mission; see [14] for the mission specific design and [59] for laying the groundwork for the crossed dipole antenna to radiate optimally at approximately 400 MHz.

While [14] and [59] utilized *Altair's* CADFEKO antenna modeling and simulation software, this work introduces antenna modeling, analysis, and design using MATLAB's Antenna Toolbox. The Antenna Toolbox gives designers popular antenna models to build and adjust based on required application parameters. Figure 29 shows the crossed dipole antenna design constructed MATLAB's Antenna Toolbox, and Figure 30 shows the antenna with its anticipated 3-D radiation pattern at 401.08 MHz. Figure 31 shows the 2-D azimuth radiation pattern of the crossed dipole antenna including a 3dB or Half-Power Bandwidth (HPBW) value of 128°. We can see from Figures 30 and 31 that the crossed dipole antenna achieves an omni-directional pattern as intended with a 2.1 dBi maximum antenna gain. From Figure 29, we can gather the physical dimensions of the design as well. Finally, Figure 32 shows the impedance value in terms of resistance and reactance for the modeled crossed dipole antenna. All these parameters are extracted from Figures 29 through 32 and compiled in Table 18.

TABLE 18: 401.08 MHz UHF Antenna MATLAB Design Parameters

Element Length (4 total)	175.6 mm
Element Diameter	7.5 mm
Antenna Gain	2.1 dBi
3dB/HF BW	128°
Active Impedance	$71.0 - j3.8\Omega$

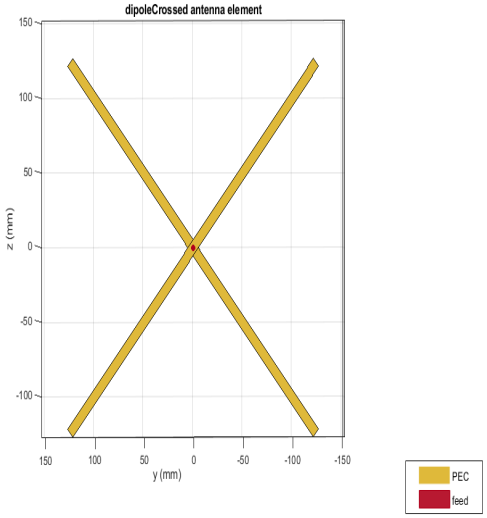

Fig. 29: Crossed Dipole Antenna Design in MATLAB's Antenna Toolbox

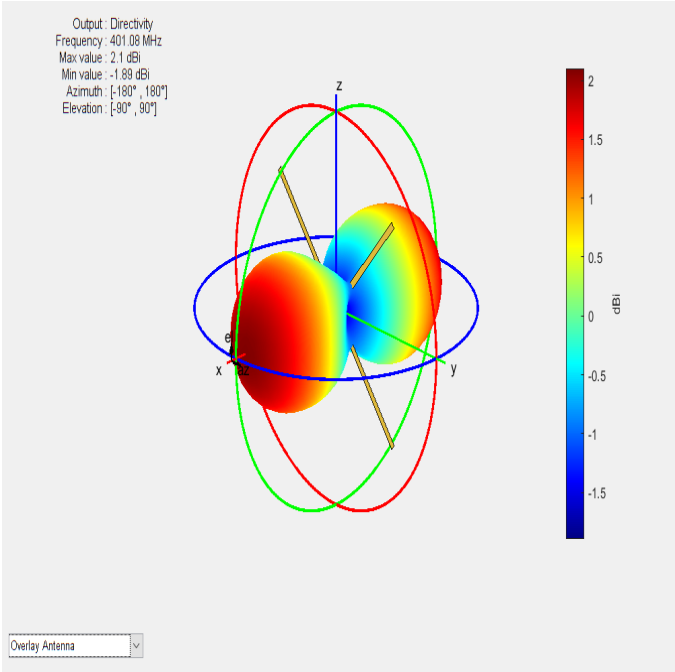

Fig. 30: Crossed Dipole Antenna 3-D Radiation Pattern at 401.08 MHz

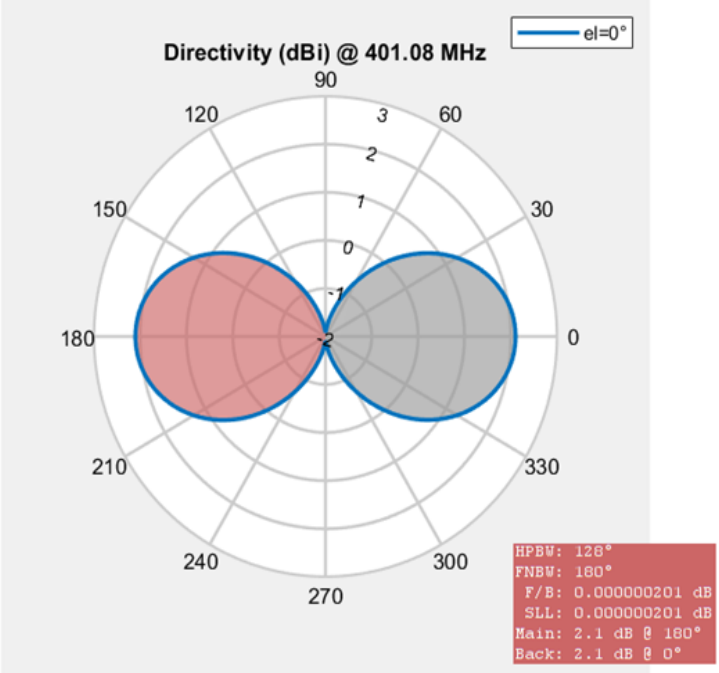

Fig. 31: Azimuth (2-D) Radiation Pattern of Crossed Dipole Antenna at 401.08 MHz

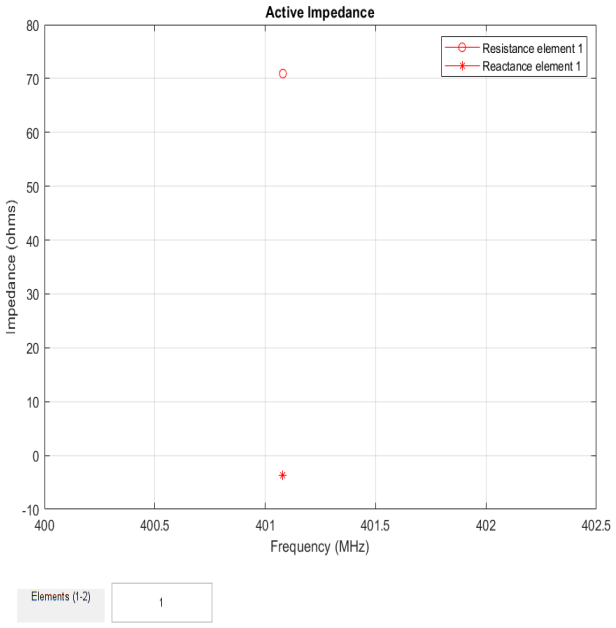

Fig. 32: Active Impedance for Crossed Dipole UHF Antenna

The MATLAB Antenna Design software reduced the electrical length based on the design parameters to minimize the reactance of the input impedance. The designed impedance does not have zero reactance, but it is a significant improvement from 42.2Ω original reactance value and that will contribute to radiating power more efficiently. The negative sign of the new reactance indicates that the length of the elements are slightly short of the ideal length since a capacitive reactance is experienced as shorter than resonant lengths for dipoles [58]. This is also supported by the theory shown before since the software simulated length is 2 mm shorter than the 95% length in (34). This can be easily adjusted, tested, and verified when constructing the physical antenna for SeaLion to ensure the minimum reactance is obtained.

At the time of this writing, the S-Band antenna selected for SeaLion is the COTS GOMSpace AM2150 Antenna System. This system will consist of two opposing directional patch antennas to create an omni-directional radiation pattern of S-band radio frequency. The GOMSpace single S-band patch antenna is shown in Figure 33 while the two opposing antennas with their radiation patterns are shown in Figure 34 on a generic CAD CubeSat extracted from the manufacturer's datasheet [8].

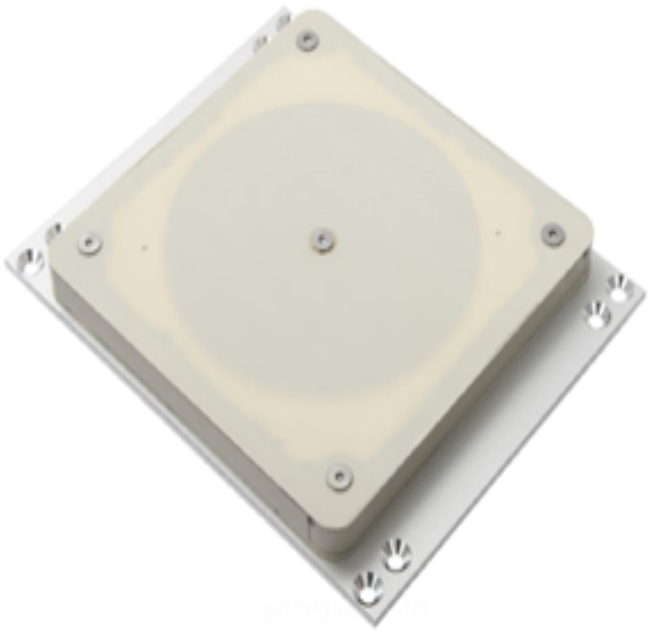

Fig. 33: GOMSpace AM2150 S-band Patch Antenna

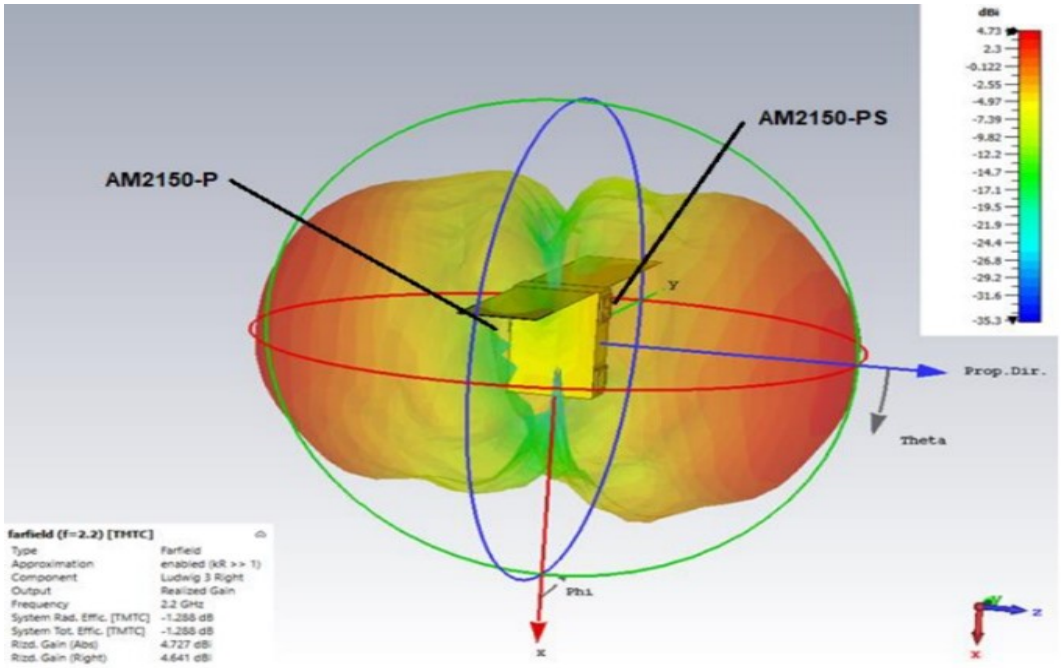

Fig. 34: 3-D Radiation Pattern of Opposing AM2150 S-band Patch Antennas from [8]

4.4 RADIO LINK BUDGET ANALYSIS

The radio link budget must be derived and verified to ensure SeaLion has the ability to wirelessly communicate with the selected ground stations while in orbit. Transmitted and received power, antenna gains, and losses must all be accounted for to ensure data can be effectively communicated between the ground and the satellite. [60] provides the theory and layout for calculating the necessary values and establishing and effective radio link budget for a CubeSat. With the limited power available at the satellite radio receiver, the Signal-to-Noise (SNR) ratio at SeaLion must be sufficient in order to decode message symbols transmitted from the ground station. The SNR is calculated by taking the ratio of the energy per bit, E_b, to the noise spectral density.

$$SNR = \frac{E_b}{N_0} = \frac{P_r}{N_0 R} \tag{35}$$

where $E_b = \frac{P_r}{R}$ and is the ratio of the received power, P_r, to the data rate, R, in bits per second (bps), that the radio link is intended to support [60]. The noise spectral density, N_0, is calculated using the Boltzmann's constant, k, and the antenna noise temperature T_{ant} and receiver noise temperature, T_r, resulting in (36).

$$N_0 = k(T_{ant} + T_r) \tag{36}$$

The received power is the function of the power at the transmitter, P_t, transmitter gain, G_t, receiver gain, G_r, and the propagation loss, L_p. The power received can be calculated with these values using [60].

$$P_r = \frac{P_t G_t G_r}{L_p} \tag{37}$$

where L_p, or the free-space path loss (FSPL), is the power lost while the signal travels through free space and is driven mainly by the distance the signal has to travel. The L_p is determined by [60].

$$L_p = (4\pi d \frac{f}{c})^2 \tag{38}$$

and d is the distance between the transmitter and the receiver. From the orbital analysis completed by SeaLion team members, the maximum distance that SeaLion will be from the ODU ground station while in line of sight is 1578.3 km which corresponds to a free-space path loss of 148.5 dB. The maximum distance from the CGA ground station while in line of sight is 1516.5 km which corresponds to a FSPL of 162.24 dB for the S-Band

uplink and a FSPL of 163.03 dB for the S-Band downlink. Combining (35), (36), (37), and (38) we can now find the "minimum SNR required to ensure reliable communication for a specified data rate R." [60] This is dependent on the bit error rate (BER) of a specific modulation scheme [55] and in this case it is dependent on GMSK modulation, which is a type of coherent binary FSK. Per [14], [60] designs, for reliable radio communications, a BER maximum of 10^{-5} should be selected. This corresponds to a minimum SNR of 10 dB to ensure reliable communication. The link margin is a radio link budget parameter that shows the dB difference between the minimum required SNR and the anticipated SNR [61]. The link margin shows at what point the SNR is not great enough to overcome the noise and losses in the radio link system. It is useful to establish bounds on link margin for a radio link budget since it is also a function of distance and therefore free-space path loss. Tables 19 and 20 shows the full radio link budgets for UHF and S-band links, respectively. Note, receiver noise temperature and antenna noise temperature used in (36) are estimates for both frequency bands; see [14], [60] on the derivation of these values. The S-band ground station power and antenna gain values were extracted from the MC3's User Guide [52]. These link budgets show that even for the maximum distance SeaLion will be to the ground stations, there is sufficient SNR to reliably communicate and, thus, there will be for the entirety of the mission duration.

TABLE 19: SeaLion Radio Link Budget for UHF Communications with ODU Ground Station

	Uplink	Downlink
Frequency	401.08MHz	401.08MHz
Transmit Power P_t	13.98 dBW	0 dBW
Transmit Antenna Gain G_t	16.48 dBi	2.15 dBi
FSPL	148.5 dB	148.5 dB
Connector Losses	3.6 dB	3.6 dB
Receive Antenna Gain G_r	2.15 dBi	16.48 dBi
Reciever Noise Temp T_r	2610 K	855 K
Antenna Noise Temp T_{ant}	290 K	150 K
System Noise Temp T_s	2900 K	1005 K
Data Rate R	9600 bps	9600 bps
Received SNR	34.69 dB	28.42 dB
Required SNR for 10^{-5} BER (GMSK)	$\geq$ 10 dB	$\geq$ 10 dB
Link Margin	$\leq$ 24.69 dB	$\leq$ 18.42 dB

TABLE 20: SeaLion Radio Link Budget for S-Band Communications with CGA Ground Station

	Uplink	Downlink
Frequency	2037.5MHz	2232.5MHz
Transmit Power P_t	14.77 dBW	-1.55 dBW
Transmit Antenna Gain G_t	35 dBi	4.73 dBi
FSPL	162.24 dB	163.03 dB
Connector Losses	3.6 dB	1.5 dB
Receive Antenna Gain G_r	4.73 dBi	35 dBi
Reciever Noise Temp T_r	2610 K	855 K
Antenna Noise Temp T_{ant}	290 K	150 K
System Noise Temp T_s	2900 K	1005 K
Data Rate R	76800 bps	76800 bps
Received SNR	33.78 dB	23.37 dB
Required SNR for 10^{-5} BER (GMSK)	$\geq$ 10 dB	$\geq$ 10 dB
Link Margin	$\leq$ 23.78 dB	$\leq$ 13.37 dB

CHAPTER 5

CONCLUSION

In this work, the 3U Mission SeaLion CubeSat led by ODU's Space Systems students was introduced. For this mission, I proposed a custom in-house EPS design and verified chosen and custom radio communications hardware with simulation modeling and link budget analysis. A review of popular COTS available modules was first conducted to evaluate typical EPS performance characteristics and notable features to design a comparable module in-house. To optimize SeaLion's brief time in viable orbit, I proposed using novel primary non-rechargeable battery cells as the satellite's one and only source of electrical power. In the EPS design, great emphasis was placed on the electrical power conversion, specifically on the DC-DC voltage converter, in order to properly distribute appropriate voltage and current to the payload and mission operations electronics. Through theory, analysis, and software simulation, the DC-DC converter performance and component selection were verified. The custom EPS design proposed shows the feasibility of reducing complexity for mission lifetime and budget constrained space missions while still providing the team a high probability of successfully completing the mission objectives. For the radio communications, the in-house UHF antenna design was verified through theory and software modeling and simulation. A link budget analysis was conducted of uplink and downlink communications for both UHF and S-band frequencies, and SNR at the receiver was sufficient for reliable radio communications throughout the mission lifetime.

5.1 FUTURE WORK

As expected, future work for Mission SeaLion lies in fabrication and testing of chosen and designed subsystems. The EPS PCB fabrication will enable testing in each portion of the design covered in this thesis. ODU Space Systems Lab's recent acquisition of a vacuum chamber will enable swift and thorough testing of the EPS and its associated components. As described in this work, the battery cells, voltage regulators, and other ICs' performances are intended to operate in specific temperature ranges. Being able to verify these components and designed circuits' performance in variable real-world temperatures will increase their reliability and the overall likelihood of SeaLion's mission success. Additionally, the in-house

designed UHF antenna will be fabricated and tested to verify the software model generated in this thesis. After an approved FCC experimental radio license is secured, the radio hardware will be tested to verify a radio link can be reliably established. After fabrication and testing of the EPS and communications equipment, these subsystems will be ready for service onboard Mission SeaLion.

REFERENCES

[1] W. Larson and J. Wertz, *Space Mission Analysis and Design*, 3rd ed. El Segundo, CA: Microcosm Press, 2005.

[2] "What are smallsats and cubesats?" [Online]. Available: https://www.nasa.gov/content/what-are-smallsats-and-CubeSats, accessed: Apr. 4, 2022.

[3] GOMSpace, "Gomspace p31u module datasheet," https://gomspace.com/shop/subsystems/power/nanopower-p31u.aspx, accessed: Feb. 2, 2022.

[4] R. Burt, "Distributed electrical power system in cubesat applications," Master's thesis, Utah State University, 2011.

[5] P. Fortescue, G. Swinerd, and J. Stark, *Spacecraft Systems Engineering*, 4th ed. The Atrium, Southern Gate, Chichester, West Sussex, PO19 8SQ, United Kingdom: Wiley, 2011.

[6] D. Linden and B. Reddy, *Handbook of Batteries*, 2nd ed. New York, NY: McGraw-Hill, 2002.

[7] UltraLife Corporation, "UHR-XR34610 Datasheet," [Online]. Available: https://www.ultralifecorporation.com/ECommerce/product/uhr-xr34610-cell/3v-li-cfx-mno2-hybrid-non-rechargeable-d-cell, accessed: Sep. 20, 2021.

[8] GOMSpace, "GOMSpace AM2150 Antenna System Datasheet," https://gomspace.com/shop/subsystems/communication-systems/nanocom-am2150.aspx, accessed: Feb. 1, 2022.

[9] "Cubesat 101: Basic concepts and processes for first-time cubesat developers," https://www.nasa.gov/sites/default/files/atoms/files/nasa_csli_cubesat_101_508.pdf, accessed: Apr. 4, 2022.

[10] *CubeSat Design Specification*, 14th ed., California Polytechnic State University, San Luis Obispo, CA, February 2022.

[11] M. Swartwout, "Reliving 24 years in the next 12 minutes: A statistical and personal history of university-class satellites," *32nd Annual AIAA/USU Conference on Small Satellites*, no. paper SSC18-WKVIII-03, August 2018.

[12] Virginia Space, "Thinsat program," https://vaspace.org/33/, accessed: Apr. 4, 2022.

[13] EnduroSat, "3u solar panel," [Online]. Available: https://www.endurosat.com/cubesat-store/cubesat-solar-panels/3u-solar-panel-xy/, accessed: Sep. 15, 2021.

[14] A. G. Cappiello, "Design, implementation, and analysis of electrical system architecture for cubesat to ground communications," Master's thesis, Old Dominion University, 2019.

[15] ClydeSpace, "Optimus-80," https://satsearch.co/products/aac-clyde-optimus-80, accessed: Sep. 15, 2021.

[16] FuelCellStore, "Pem fuel cells for drones, uavs, and robotics," https://www.fuelcellstore.com/fuel-cell-stacks/uav-fuel-cell-stacks, accessed: Mar. 1, 2022.

[17] G. Plett, *Battery Managment Systems Volume I, Battery Modeling*, 1st ed. Norwood, MA: Artech House, 2015.

[18] EaglePicher, "LCF-137 Datasheet," https://www.eaglepicher.com/sites/default/files/LCF-137.pdf, accessed: Sep. 20, 2021.

[19] EaglePicher Technologies, "LCF-143 Datasheet," https://www.eaglepicher.com/sites/default/files/LCF-1431120.pdf, accessed: Sep. 20, 2021.

[20] "Lithium Carbon Mono-fluoride/Manganese Dioxide Hybrid Application Guide," https://www.ultralifecorporation.com/ECommerce/product/uhr-xr34610-cell/3v-li-cfx-mno2-hybrid-non-rechargeable-d-cell, accessed: Sep. 20, 2021.

[21] EaglePicher Technologies, "Lithium Carbon Monofluoride (CFx) and LiCFx-MnO2 Hybrid," [Online]. Available: https://www.eaglepicher.com/technology/battery-chemistries/lithium-carbon-monofluoride-cfx-and-licfx-mno2-hybrid/, accessed: Sep. 25, 2021.

[22] EaglePicher Technologies, "Product Development Insight: How to Select a Non-Rechargeable Battery Pack," *EaglePicher White Papers*, February 2019.

[23] United States Army C5ISR, "Ba-5790 battery," [Online]. Available: https://c5isr.ccdc.army.mil/news_and_media/BA_5790_Battery/, accessed: Mar. 5, 2022.

[24] J. Warner, *The Handbook of Lithium-Ion Battery Pack Design*, 2nd ed. Waltham, MA: Elsevier, 2015.

[25] UltraLife Corporation, "UHR-XR34610 Safety Datasheet," [Online]. Available: https://www.ultralifecorporation.com/ECommerce/product/uhr-xr34610-cell/3v-li-cfx-mno2-hybrid-non-rechargeable-d-cell, accessed: Sep. 20, 2021.

[26] N. Mohan, *Power Electronics: A First Course*, 1st ed. Hoboken, NJ: Wiley, 2012.

[27] Texas Instruments, "LM2576 SIMPLE SWITCHER® 40V, 3A Low Component Count Step-Down Regulator," https://www.ti.com/product/LM2576, accessed: Sep. 1, 2021.

[28] Microchip Technology, Inc., "Lm2576 52 khz simple 3a buck regulator," [Online]. Available: https://ww1.microchip.com/downloads/en/DeviceDoc/LM2576-52kHz-Simple-3A-Buck-Regulator-DS20006238A.pdf, accessed: Sep. 1, 2021.

[29] B. Lynch and K. Hesse, "Under the Hood of Low-Voltage DC/DC Converters," *Texas Instruments Power Supply Design Seminar*, 2002.

[30] P. Shenoy and A. Fagnani, "Common Mistakes in DC/DC Converters and How to Fix Them," *Texas Instruments Power Supply Design Seminar*, 2018.

[31] N. Mohan, T. Undeland, and W. Robbins, *Power Electronics: Coverters, Applications, and Design*, 2nd ed. Hoboken, NJ: Wiley, 1995.

[32] Vishay, "Solid Tantalum Chip Capacitors, TANTAMOUNT™, Ultra-Low ESR, Conformal Coated, Maximum CV," https://www.vishay.com/docs/40047/597d.pdf, accessed: Jan. 2, 2022.

[33] M. Score, "Ceramic or electrolytic output capacitors in DC/DC converters—Why not both?" *Texas Instruments Analog Applications Journal*, April 2015.

[34] Electrocube, "Technical Bulletin No. 03: Why Do Capacitors Fail?" https://www.electrocube.com/pages/why-capacitors-fail-technical-bulletin, accessed: Oct. 21, 2021.

[35] J. Rittenhouse and J. Singletary, *Space Materials Handbook SP-3025: Supplement 1 to the Second Edition*, 2nd ed., National Aeronautics and Space Administration, Washington, D.C., January 1966.

[36] S. Arnold, J. Armstrong, C. Person, and M. Tietz, "QbX - The CubeSat Experiment," *26th Annual AIAA/USU Conference on Small Satellites*, 2012.

[37] B. C. de V. Sheard, "An electrical power system for cubesats," Master's thesis, University of Cape Town, 2015.

[38] N. Ya'acob, M. F. Ayob, and N. Tajudin, et al., "Single event latch-up detection fornano-satellite external solar radiation mitigation system," *Bulletin of Electrical Engineering and Informatics*, vol. 10, no. 1, pp. 39–45, February 2021.

[39] L. T. Lumbwe, "Development of an onboard computer (obc) for a cubesat," Master's thesis, Cape Peninsula University of Technology, 2013.

[40] N. Singh, N. Raman, J. Parikh, and V. Goradia, "Hardware Architecture Of Electrical Power System For 3U Hyperspectral Imaging Cubesat," *70th International Astronautical Congress (IAC), Washington D.C., United States*, October 2019.

[41] R. Borowicz, "Failure mode, effects, and critical analysis of very low earth orbit 3u cubesat," Master's thesis, Old Dominion University, 2022.

[42] Analog Devices, "LTC4361-1/LTC4361-2 Overvoltage/Overcurrent Protection Controller," https://www.analog.com/media/en/technical-documentation/data-sheets/LTC4361-1-4361-2.pdf, accessed: Jan. 4, 2022.

[43] J. Wertz, D. Everett, and J. Puschell, *Space Mission Engineering: The New SMAD*, 1st ed. Hawthorn, CA: Microcosm Press, 2011.

[44] N. Nise, *Control Systems Engineering*, 7th ed. Wiley, 2015.

[45] Analog Devices, "LTC2944 60V Battery Gas Gauge with Temperature, Voltage and Current Measurement," [Online]. Available: https://www.analog.com/media/en/technical-documentation/data-sheets/2944fa.pdf, accessed: Sep. 25, 2021.

[46] Analog Devices, "LTC2990 Quad I2C Voltage, Current and Temperature Monitor," [Online]. Available: https://www.analog.com/media/en/technical-documentation/data-sheets/LTC2990.pdf, accessed: Jan. 4, 2022.

[47] N. Daniels, *NanoRacks External CubeSat Deployer (NRCSD-E) Interface Definition Document (IDD)*, 1st ed., NanoRacks, LLC., Webster, TX, August 2018.

[48] J. S. Harris, "Analysis and implementation of communications systems for small satellite missions," Master's thesis, Old Dominion University, 2014.

[49] Z. Leffke, J. Black, and K. Shinpaugh, et al., "A Prototype Virginia Ground Station Network," *Proceedings of the Small Satellite Conference*, p. Technical Session X: Ground Systems, August 2020.

[50] GOMSpace, "GOMSpace NanoCOM AX100 UHF Transceiver Datasheet," https://gomspace.com/shop/subsystems/communication-systems/nanocom-ax100.aspx, accessed: Aug. 10, 2021.

[51] W. Beech, D. Nielsen, and J. Taylor, *AX.25: Link Access Protocol for Amateur Packet Radio*, 2nd ed., Tucson Amateur Packet Radio Corporation, PO BOX 852754 Richardson, TX 75085-2754, July 1998.

[52] *Mobile CubeSat Command and Communications (MC3) User's Guide*, 15th ed., MC3 Network Operations Center (NOC), Monterey, CA 93943, October 2021.

[53] GOMSpace, "GOMSpace NanoCOM AX2150 S-Band Transceiver Datasheet," https://gomspace.com/shop/subsystems/communication-systems/nanocom-ax100.aspx, accessed: Aug. 26, 2021.

[54] J. Proakis and M. Salehi, *Digital Communications*, 5th ed. New York, NY: McGraw-Hill Higher Education, 2008.

[55] S. Haykin, *Digital Communication Systems*, 1st ed. Hoboken, NJ: Wiley, 2014.

[56] Z. J. Leffke, "Distributed ground station network for cubesat communications," Master's thesis, Virginia Polytechnic Institute and State University, 2013.

[57] N. Chahat, *CubeSat Antenna Design*, 1st ed. Piscataway NJ: Wiley IEEE Press, 2021.

[58] T. Milligan, *Modern Antenna Design*, 2nd ed. Hoboken, NJ: Wiley-Interscience IEEE Press, 2005.

[59] J. Harris, W. Kim, M. O'Brien, and D. Popescu, "Adapting a Commercial-Off-The-Shelf Amateur Radio Antenna for Use in Small Satellite Ground Station Radio Link," *Antenna Measurement Techniques Association*, November 2018.

[60] O. Popescu, "Power Budgets for CubeSat Radios to Support Ground Communications and Inter-Satellite Links," *IEEE Access*, vol. 5, pp. 12 618–12 625, July 2017.

[61] T. Pratt, C. Bostian, and J. Allnutt, *Satellite Communications*, 2nd ed. Hoboken, NJ: John Wiley and Sons, 2003.

APPENDIX A

COPYRIGHTS

The following copyright permissions were obtained for legal reproduction or adaptation of previously published figures for use in this work:

The graphic for Figure 6 comes from a publication by Fortescue, Swinerd, and Stark [5].

The graphic for Figure 7 comes from a publication by Linden and Reddy [6].

The data in Table 3 is an adaptation from a table in a publication by Larson and Wertz [1].

The permission receipts are included on the following pages.

Order Number: 1207117
Order Date: 04 Apr 2022

Print order

Payment Information

Joseph Siciliano
jsici001@odu.edu
Payment method: Invoice

Order Details

1. Space mission analysis and design

Billing Status: Open

Print License

Order License ID	1207117-1	**Type of use**	Republish in a thesis/dissert...
Order detail status	Completed	**Publisher**	KLUWER ACADEMIC PUBLIS...
ISBN-13	9780792359012	**Portion**	Chart/graph/table/figure

0.00 USD
Republication Permission

View Details

Publisher Terms and Conditions

2. Spacecraft Systems Engineering

Billing Status: Open

Print License

Order License ID	1207117-2	**Type of use**	Republish in a thesis/dissert...
Order detail status	Completed	**Publisher**	Wiley
ISBN-13	9780470750124	**Portion**	Chart/graph/table/figure

0.00 USD
Republication Permission

View Details

Publisher Terms and Conditions

Total Items: 2

Subtotal: 0.00 USD
Order Total: 0.00 USD

Handbook of batteries

GENERAL INFORMATION

Request ID	600076091	**Request Date**	04 Apr 2022
Request Status	Accepted	**Price**	0.00 USD Special Terms

ALL DETAILS

COMMENTS

Add Comment / Attachment

04 Apr 2022 6:00:17 AM, by Joseph Siciliano

Use figure (with credit to authors) in university thesis

VITA

Joseph D. Siciliano
Department of Electrical and Computer Engineering
Old Dominion University
Norfolk, VA 23529

EDUCATION

Bachelor of Science Electrical Engineering
United States Coast Guard Academy May 2018
New London, CT

PUBLICATIONS

P. Swaszek, R. Hartnett, K. Seals, J. Siciliano, R. Swaszek, "Limits on GNSS Performance at High Latitudes," *Proceedings of the 2018 International Technical Meeting of The Institute of Navigation*, Reston, Virginia, January 2018, pp. 160-176.

Typeset using LaTeX.